



Järnvägsgruppen

BOMBARDIER

Front Shape and Slipstream for Wide Body Trains at Higher Speeds

Astrid Herbst

Tomas Muld

Gunilla Efraimsson

KTH Railway Group

Publication 1402

ISBN 978-91-7595-057-0

Gröna tåget
Slutrapport" Frontform och vinddrag för breda tåg i höga hastigheter"

Engelska: Green train - Front shape and slipstream for wide body trains at higher speeds

Astrid Herbst, Tomas Muld, Gunilla Efraimsson

Table of Contents

1. Summary	3
2. Introduction	4
3. Full-Scale Measurements.....	8
4. Simulations using efficient analysis technique	12
Verification and validation of methods to identify flow structures	12
Impact of carbody width on slipstream evaluation following TSI	15
Impact of tail geometry on slipstream flow structures	17
Comparing flow structures from POD and DMD	21
Impact of train length on wake flow pattern.....	24
5. Aerodynamic optimization.....	27
6. New improved front end design	33
7. Conclusions	39
Publications.....	41
Exchange of knowledge via conferences, seminars, courses and cooperation.....	42
References	44

1. Summary

New requirements on slipstream air speeds and head pressure pulse in the revised Technical Specification for Interoperability (TSI) for train speeds higher than 190 km/h are more difficult to fulfill for wide body trains and high trains. The requirements are derived from experiences from trains with UIC-profile, not representing Swedish conditions. The objective of the project was to increase the knowledge about slipstream air flow of wide body trains at higher speeds, understand the implications of the new requirements on the front shape and to develop a prediction methodology in order to take this into account early in the design cycle. The front design was in parallel optimized with respect to head pressure pulse and drag. The starting point was the Regina train.

The project started in August 2007, even though the contract was signed first in November 2007. The contract regarding the continuation of the project was signed in April 2010. The project was finalized 2012.

Svenska: Sammanfattande projektbeskrivning

Nya krav på inducerat vinddrag och tryckpulser (på omgivningen) i TSD för tåg med hastighet över 190 km/h är svårare för breda tåg och höga tåg att klara. Nivåerna är anpassade till erfarenheter med tåg på kontinenten med UIC-profil och inte efter svenska förhållanden. Projektet syftade till att öka på kunskapen om inducerat vinddrag från breda tåg i höga hastigheter, förstå vilka implikationer de nya kraven har på tågfrontens utformning (i positionen längst bak) och utveckla en predikteringsmetodik för att kunna ta in dessa hänsyn tidigt i designcykeln. Variationer i frontens geometri utvärderades och optimerades också med avseende på tryckpulser och luftmotstånd. Studierna utgick från Regina 250.

Projektet har påbörjats i augusti 2007, även om avtal först undertecknades i november 2007. Avtal om projektets fortsättning har slutits april 2010. Projektet slutfördes 2012.

2. Introduction

A moving train pulls the air along the train resulting in a so-called slipstream which can be felt and measured as an air movement also a short distance away from the train. Modern trains at higher speeds are relatively smooth and the highest wind speeds occur in a train's wake where the nature of the flow is strongly linked to the front shape (when operating as rear). A train's front passing by generates an increase in pressure in front of it and a decrease in pressure at the sides of the nose. Therefore due to the changing pressure levels, pressure loads e.g. on the surrounding infrastructure of the track will be generated. Both the slipstream and the pressure pulses from passing trains give rise to forces on the surroundings which increase with the running speed. For track-side workers and people and objects on an adjacent platform it is therefore due to safety reasons necessary to limit the induced air velocity and pressure pulse (see e.g. Figura-Hardy (2007) [7]) When the train passes a station, it needs to be ensured that people neither stumble nor fall nor items like strollers start rolling.

Within the audit progress of the Technical Specification for Interoperability (TSI) [1], requirements regarding the maximum air velocities at the side of a train and in its wake have been introduced. These consist of different criteria with respect to the safety of workers and people on the platform. As for the slipstream, the revised TSI contains new requirements on pressure pulses. The allowed levels can also be subject to further restrictions due to specific requirements of the operator.

The requirement levels in the TSI regarding slipstream and head pressure pulse have been developed on the principle that new trains should not give more impact than existing trains. Experiences regarding trains at higher speeds are primarily based on trains with UIC profile. The measurement points where these TSI requirements must be met are specified from the center of track not taking into account the actual profile. Since the measurement points are defined from center of track, it will be challenging for wide body trains making use of the entire gage in Sweden and Finland to meet the requirements and the impact of these requirements on the shape of the rear of a train increases. Measurements on double deck trains in Germany indicate that even for higher trains, double deck trains, meeting the slipstream requirements at higher speeds is an issue. Prior to this project, very little knowledge existed on the level of head pressure pulses and slipstream of Swedish trains under Swedish conditions, and what it means for increasing the speed to 250 km/h and above.

The formulation of the requirements in the revised TSI is a compromise between countries who want a lower level, such as Germany and the UK, and others who want a higher level, such as Finland, although e.g. Bombardier would have liked to go for higher values given measured values for a double deck trains in Germany and given the wide body trains in Sweden. Germany and the UK would not allow higher air speeds than those for which operation is regarded as safe based on the existing experience. One obvious problem in the argument for higher values, which are better suited for Sweden and Finland, is the lack of documentation about the phenomenon under Swedish conditions. The project contributes to increase the knowledge regarding slipstream and head pressure pulse under the specific Scandinavian conditions.

The "Gröna tåget" (Green Train) has been initiated by Banverket (later Trafikverket) which is the sector authority in the rail transport area in Sweden. Banverket's R&D program stated that the "Gröna Tåget" supports collaboration with manufacturers of vehicles and other equipment in terms of R & D efforts to develop and maintain skills for construction of railway equipment specifically suited for Swedish conditions." In the first place, the program aimed at creating opportunities to develop and procure the next generation of high speed trains (the successor to the X2000), for speeds of 250 km/h and above (see Fröidh (2012) [8] for reference).

Therefore the focus of this project regarding aerodynamics within the framework of Gröna tåget was not only to increase the knowledge of slipstream air flow of wide body trains at higher speeds with full scale measurements as a starting point and understand the implications of the new requirements on the front shape but to develop a prediction methodology in order to take slipstream into account early in the design cycle of a train. The final design of a train is an optimization balancing various requirements. Legal specifications like the TSI regulations on head pressure pulse and slipstream outlined above ensuring the health of passengers and staff as well as interoperability between different countries must be obeyed. Further, requirements can originate from specific customer requests which in their turn are formulated to meet the requirement of the transport market in a specific region.

Designing the outer shape of a train has major impact on the aerodynamic performance of a vehicle (see e.g. Schetz (2001) [19] for further reading on train aerodynamics). The shape of the front that gives low pressure pulses is not necessarily the one which gives low induced velocities in the slipstream, why it is important to evaluate front shapes for both of these phenomena. The front shape is also important for drag - which gives a significant contribution to the energy consumption at higher speeds and crosswind safety, i.e. the ability to withstand high wind speeds (see e.g. Baker et al. (2011) [3], (2009) [4] and Diedrichs (2009)[5], (2010)[6]). In addition, other demands on the front which are related to the crash structure, viewing angles and length available for passengers restrict its development.

The final goal is to generate a design which has a good performance both with respect to the slipstream generated behind the train and with respect to the pressure distribution around the front because the front for most modern trains can be operating as the rear as well. Besides the safety related issues, the optimization of the geometry of a train with respect to drag, slipstream and head pressure pulse gives a positive contribution to the environment. For trains at higher speeds, drag contributes significantly to the train resistance and is therefore contributing to minimizing energy consumption. Improving the performance with respect to slipstream has significant impact on the aerodynamic drag. Reducing aerodynamic drag saves up to 15 percent of the energy in high speed trains. Limiting drag and maximizing stability also increase acceleration which reduces traveling time.

Traditionally, a way of exploring the set of design modifications with regard to their aerodynamic performance has been to check them experimentally in the wind tunnel. Here the iterative development of further designs is based on theory and engineering skills. However, this approach is rather costly and time consuming. Further, in many cases due to the large number of possible designs it is unlikely that the truly optimal design can be found without assistance of automatic tools. The increasing performance and price drop of today's computers facilitate the use of modern CAE based optimization tools for

determining the optimal parameters for the external shape of trains. A system was developed that helps to optimize the aerodynamic performance of rail vehicles using state-of-the-art computer-aided engineering (CAE) tools.

For the prediction of pressure pulses occurring during the passage of the front of a train, a well-established methodology exists. For a streamlined train, inviscid Euler equations can be solved quickly with Panel methods or slightly more costly solving the Reynolds averaged Navier-Stokes (RANS) with commercial software. For slipstream due to the non-steady turbulent flow in the wake of the train, the development of a prediction methodology is a much more challenging task. Prior to this project, estimates were made using simpler calculation methods (RANS) and experiments in wind or water tunnel. In the wind tunnel, the ground is usually not in motion which changes the flow. Even for a wind tunnel facility with a moving belt, the width of the belt and the speed at which it is moving is limited. Using water tunnel tests many runs are needed to get enough statistical data. Therefore the method is not so well suited to make more extensive parameter studies. An alternative facility is presented in Gil et al. (2008), where a train model is mounted on a rotating rig. Verification by full scale measurements can only be carried out on an already built train. In order to take this into account early during the design cycle of the train and to reduce the impact on the environment in a design cycle, an effective prediction method is required which did not exist prior to this project. Large eddy simulation (LES) is a method that gives a sufficient accuracy and is the starting point. It is unfortunately time and computationally intensive. For trains at higher speeds for which “Gröna Tåget” aims at, it is important to be able to predict the slipstream phenomenon to ensure that the requirements of the TSI are met. In order to take into account the slipstream effect in design cycle for front design, it is important to get a better understanding of the link between the front shape and the slipstream, and a computationally efficient prediction methodology.

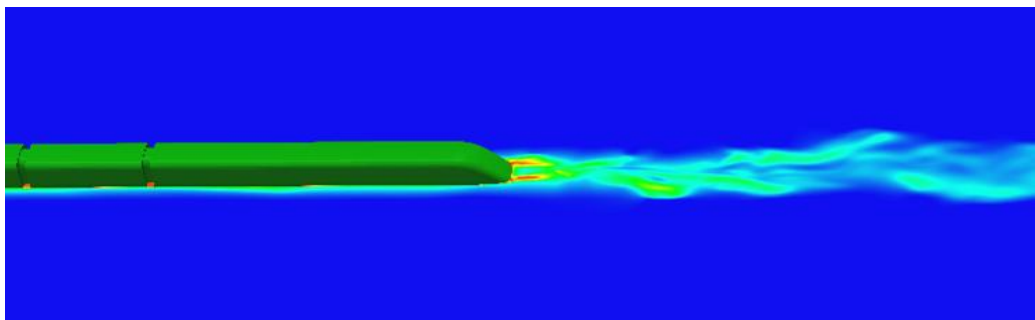


Figure 1 Visualization of the air flow along and behind the train, as computed with CFD methodology

During the course of the project, a solid understanding of how the turbulence modeling technique should be used for calculations of the structures in the wakes to get reliable calculation results has been acquired. Detached eddy simulation (DES) has shown promising results (Spalart (1997) [21], (2006)[22]). DES is a computationally a less intensive method than Large eddy simulation (LES) (see Sagaut et al. (2006)[18], applied to train aerodynamics Hemida & Baker (2011)[10]). Furthermore, we have implemented and evaluated the analysis based on the so-called proper orthogonal decomposition (POD) (see Lumley (1967) [12]) and alternatives to those (Koopman modes, see for reference Rowley et al.

(2009) [17] and Schmid (2010) [20]). The methodology developed for the analysis of wake structures has been refined and applied to get an effective tool for analysis for the design of high-speed wide body trains for the best way to be included in the design iterations where all requirements related to the front are considered. Calculations on train geometries with different head shapes were performed and compared to the experimental data. A solid understanding of how such train length affect wake structures and thus the slipstream and with it the train's energy consumption was developed. Numerical results were supplemented with water / wind tunnel tests for verification. Shape optimization of the front was carried out and resulting front shape was tested in the wind tunnel.

3. Full-Scale Measurements

The natural starting point of the project was to gain experience on the behaviour of wide body trains regarding slipstream and head pressure pulse by carrying out experiments in full scale given the limited pre-existing data regarding the performance of wide body trains. The aim was to generate reference data for comparison with numerical results and to compare the performance to the requirements of the TSI RST HS [1]. The slipstream intensity of a modified two-car Regina train was therefore measured in a full scale track-side measurement campaign. Modifications of the external train shape pertain to bogie skirts that were mounted on one end bogie and a horizontal cover plate attached underneath the snow plough cavity. A further test objective was to assess the aerodynamic impact of the modifications mentioned above.

The test procedure to measure the slipstream velocity according to the TSI is as follows: The velocity is measured at a probe stationary to the ground, as the train passes. The probe is located 3 m from the center of the track and 1.2 m over the platform or 0.2 m over TOR for the trackside measurement. This should be done at least 20 times and each sample is filtered with 1s-moving time average. From these filtered profiles the maximum velocity from each run is obtained, which is averaged and $u_{2\sigma}$ is obtained,

$$u_{2\sigma} = \bar{u} + 2\sigma$$

where u is the maximum filtered velocity for each run, the bar indicates mean and σ is the standard deviation. The $u_{2\sigma}$ is not allowed to be higher than 15.5 m/s for the platform TSI and 20 m/s for trackside TSI for trains at operating at 200 kph. Regarding head pressure pulse, the maximum permitted pressure changes are specified in TSI HS RST : Peak-to-peak pressure change: ≤ 720 Pa at speeds below 250 km/h (795 Pa at 250 km/h), measured 2.5 m from track centre, determined as average plus two standard deviations from at least 10 tests. This must be shown for seven different heights between 1.5–3.3 m above top of rails.

The train induced slipstream air velocity was measured by means of three separate 3D-ultrasonic anemometers (USA) using a sampling rate of 260 Hz. The train velocity and position was measured by means of two sets of light barriers. The light barriers were mounted slightly above the top of one rail such that single wheel passages were detected. The light-barrier signals were recorded along with the slipstream air velocities. 21 valid passages of the test vehicle for “Gröna Tåget” have been measured. The bogie skirts were mounted on the leading and trailing bogies in 11 and 10 tests, respectively.

To evaluate the recorded data, the track parallel air velocity was corrected by the track parallel wind (Galilean transformation). The train speed is corrected by the track parallel wind (Galilean transformation). The corrected air velocities are normalised with the corrected train speed. Time is transformed into spatial positions x along the train, where $x = 0$ m is at the first axle. The transformation is based on the train speed, acceleration and the individual sensor positions (spatial offset). The recorded data is re-sampled into an equidistant grid that is distributed along the vehicle, using a closest neighbour method. The final data are reduced to intervals of [-200 m ... +800 m] measured from the first axle. The ensemble average and a corresponding standard deviation are calculated on basis of all data

sets. To be able to calculate the ensemble average, the measured data must be available at the same pre-defined longitudinal positions for each test run. Since the data is recorded as a time-series, the time stamp of each sample must be transferred into a spatial position using the measured train speed and acceleration. The resulting longitudinal position will in general not fit with a pre-defined equidistant grid. Therefore, the measured raw data must be treated such, that the data is available at pre-defined longitudinal positions of an equidistant grid.



Figure 2: Gröna Tåget train, B-car with bogie skirts.

Figure 3 shows a plot of the calculated ensemble average of the track parallel u-velocity component of the slipstream effect for both leading and trailing bogie skirts. The highest turbulence intensities occur in the near wake region 10 m to 60 m behind the tail. Thereafter, the turbulence intensity decays continually but is still distinct 500 m behind the train head (about 450 m behind the tail).

In Figure 3 the normalised track-parallel air velocity is given in addition to the u-velocity. Here the track-parallel air speed is normalised with the train speed:

$$C_{u,wind} = \frac{u_{wind}}{v_{train}} \quad (1)$$

The ensemble average is defined as follows. If the slipstream intensity has been measured n times with respect to an axial coordinate x with the origin referring to a well-defined position under the train, an average slipstream profile can be calculated between the n individual slipstream profiles. Here, n denotes the ensemble size in the sense of independent measurements. Depending on the sampling frequency, the train speed, and other constraints the slipstream intensity will be obtained at discrete locations x_k , that are constant for all data sets. The ensemble can consist of individual runs recorded by a single probe or by the recordings of several probes which are axially separated and which are placed at the same lateral and vertical positions with respect to the top of rails and centre of track.

The ensemble averages returned by using leading and trailing bogie skirts reveal a strong impact of the modifications on the slipstream intensities, as shown in Figure 3. Further, the slipstream peak in the wake of the train is significantly reduced when the bogie skirts are mounted at the rear end and the position of the maximum peak is changed to a position farther downstream. The most significant changes in the slipstream behaviour occur in a region between 60 m and 130 m behind the first axles which corresponds to about 10 m and 80 m behind the tail of the train (tail is located 51.1 m behind first axle). The reversed flow peak (negative u -velocity) about the nose is slightly more pronounced when the bogie skirts are mounted at the front-end.

The position of the inter-car gap is also visible in the measured data. This underlines the relevance of the gap design for the overall aerodynamic performance of the vehicle. For short trains such as the Gröna Tåget train, the inter-car gap has no significant impact on the slipstream performance since the slipstream behaviour is governed by the wake flow and thus, the tail shape. On long trains the aerodynamic performance of the inter-car gaps significantly affects the growth of the boundary layer and thus, the slipstream intensities. Furthermore, if the inter-car gaps strongly disturb the external flow, this implies a deterioration of the aerodynamic drag.

Data evaluation according to the TSI RST HS shows that the slipstream intensity is significantly reduced if the bogie skirts are mounted on the rear bogie. Both configurations pass the TSI-criterion with respect to the safety of trackside workers. It should be noted that, according to the TSI, the raw data is low-pass filtered with a one-second moving average filter. Maximum slipstream velocities are determined for each test run (data set) individually and usually occur at different longitudinal positions. The average slipstream velocity and standard deviation are calculated from these individual maxima. It should be kept in mind, that the current test conditions did not fulfil all requirements of the TSI. For example, the train speed must be kept within a narrow range around the vehicles top speed, which was not the case in this test campaign.

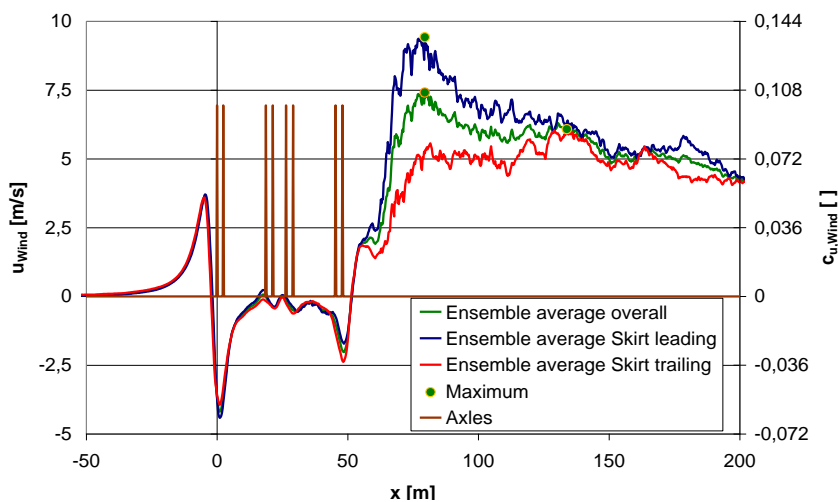


Figure 3 Measured slip stream wind speed during passage the Gröna Tåget REGINA 250 test train at the track side.

Besides the measurements regarding slipstream, even full scale tests of the head pressure pulse on the Regina 250 were performed during the project and analyzed in a Master thesis by Andre Stiebritz [T] . The focus was to study the measuring equipment to be used for measurements of the head pressure pulse according to TSI .The results of the tests were compared to numerical simulations and formed the basis for a numerical optimization regarding head pressure pulse, discussed in the section on optimization and resulting in a further master thesis by Fredrik Kållberg [M].

4. Simulations using efficient analysis technique

The need for an efficient prediction methodology for slipstream early in the design cycle and hence reduce the risk for type-testing with respect to TSI regulation was outlined in the introduction. In order to improve the relation between the shape of the front of the train and the slip stream effect, the use of Proper orthogonal decomposition (POD) and Dynamic mode decomposition (DMD) to extract the most dominant flow structures of a simulated flow in the wake of a high-speed train was evaluated within the project. POD is relatively well known in fluid mechanics whereas DMD, also known as Koopman modes, has prior to the project start never been used on such a complex geometry as a train. The ability to use decomposition methods to successfully identify dominant flow structures for an engineering geometry, is achieved by using a flow field simulated with Detached Eddy Simulation (DES), a turbulence model enabling time accurate solutions of the flows around engineering geometries. The flow structures that were identified as dominant for slipstream are associated with vortex shedding as well as bending of the counter rotating vortices. The identification of the flow structures was performed by reconstructing the flow field using the mean flow and a subset of modes. The work, which was performed at KTH, has lead to two thesis (see [B] ,[K]).

The work is presented in following manner: Starting with the validation of the decomposed modes, both validating the flow simulations and the use of decomposition methods on flow fields from simulations using DES followed by flow data to replicate TSI-slipstream measurements which has been extracted from the simulations and the effect of wide body trains on slipstream that has been investigated. The dominant flow structures and flow topologies in the wake of the train geometries studied in this project are presented and the importance of these flow structures for the slipstream. Then, the modes extracted with POD and DMD are compared in order to get a deeper understanding of each set of modes. Finally, the differences between the flow structures behind different configurations of the same train with different number of cars have been investigated.

Verification and validation of methods to identify flow structures

The flow fields from DES simulations are used as a basis for the decomposition methods. In order to ensure the validity of the modes obtained, both the DES simulations and the decomposition of DES flow fields need to be validated. The first part, to validate the numerical simulations, is a common topic and is in some way performed in almost all CFD investigation. This could, for instance, be done by comparing some interesting quantities of the flow to results from experimental studies or from other numerical simulations. To test the entire methodology, a test case is needed which even has been analyzed using mode decomposition.

The first bluff body that is studied is the surface-mounted cube. This geometry served as a test case for the methodology used in this project. The surface-mounted cube was chosen since various data exist to be used for comparison and validation, not only of the DES simulations but also for the mode decomposition using POD. Both experimental and numerical works have been used for comparison for the work on the surface-mounted cube.

The other geometries simulated during the method development are two train geometries, which are the Aerodynamic Train Model (ATM) and the CRH1, a simplified version of a wide body train developed for the Chinese market by Bombardier Transportation. The Reynolds number in the simulations based on the hydraulic diameter, the free stream velocity and the viscosity of air is 60000, for all trains and configurations. The Aerodynamic Train Model is a generic high-speed train model compliant with UIC profile in 1:50 scale. The geometry used in the simulations is based on water towing tank experiments performed at the German Aerospace Centre (DLR). In these experiments, a configuration with 4 cars, 9 intercar gaps, simplified bogies and a platform was used. The CRH1 train geometry is a simplified version of a wide body train, compared to the ATM which is compliant with the more narrow UIC profile. This geometry is based on a wind tunnel experiment performed at TU-Berlin. It is a 1.5 car model, where the front car is a dummy car, which does not have the same shape as the tail. The case simulated in this project is not meant to replicate the wind tunnel experiment, but rather to be a comparison with the ATM case. This means that the problem setup is modified from the wind tunnel setup to comply with the ATM, and hence the water tunnel experiments at DLR. There is, for instance, a moving straight ground instead of the stationary ground with splitter plate, single ballast and rails in the wind tunnel. However, there is no platform for the CRH1 simulations and the bogies are different. Pictures of the CRH1 are shown in Figure 4. It is evident that the tail of CRH1 is much steeper than that of the ATM. The angle between the vertical plane and the tail surface is approximately 50 degrees for the ATM and 33 degrees for the CRH1. Also, the tail of CRH1 is more rounded in the streamwise direction towards the lower part of the train.

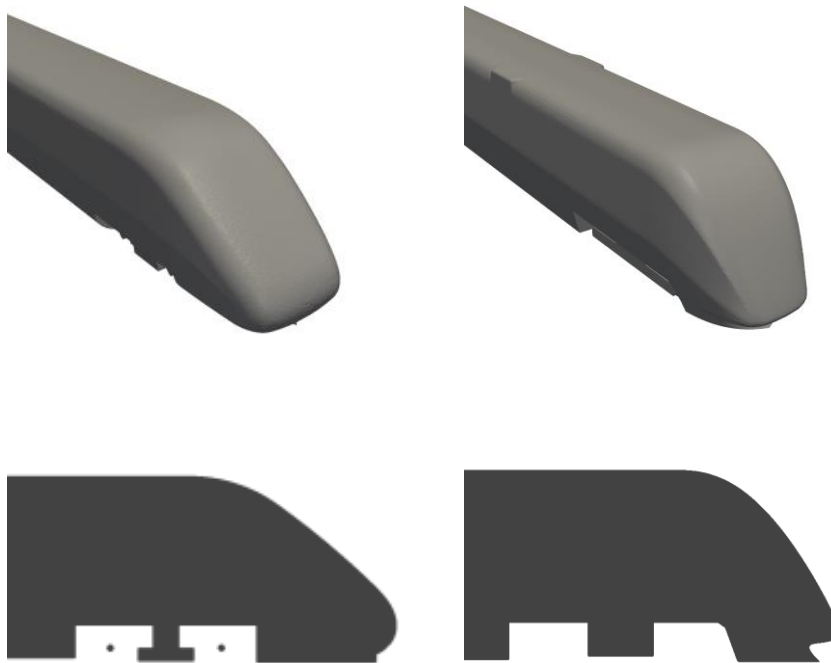


Figure 4 3- D view of the different tails and 2-D of the centerline of the simulated train geometries.

Attempts were made to validate the DES simulation results on the ATM with results from experiments performed in a water-towing tank at the German Aerospace Centre (DLR). The flow behind the ATM has been simulated with DES- $k\omega$ and compared to experimental work with Particle image velocimetry (PIV) performed at DLR (see [P]). The comparison has been done with XY-planes and velocity profiles. The comparison showed a good match in the far wake region and small discrepancies in the near wake region. When comparing the velocity profile along the side of the train, discrepancies occur along the first cars but the agreement is good towards the rear of the train. The head pressure pulse is used to align the results in the streamwise position. However, due to a trip wire in the experiments that needed to be included in the simulations, this was found to be a very cumbersome validation case. The experimental setup of the study at DLR was hard to mimic in the numerical simulations due to the trip wire. The effect of a trip wire, located on the first car in the experiments, was attempted to be modeled using a forcing function. However, it was not possible to find a forcing amplitude that gave good results throughout the domain. Instead, the work on the high-speed trains focuses on verification of the results by performing extensive grid studies, and the validation relies on the surface-mounted cube.

The feasibility of mode decomposition of a flow computed with DES was investigated ([G],[O]). The surface-mounted cube was chosen as a test case, since various data exist to be used for comparison and validation. The comparison was done with both experimental and numerical work obtained by LES simulations. The results compared well to the different studies and it was therefore found that the DES simulation contained the relevant dominant flow structures. The flow field could therefore be used to decompose into POD and DMD modes.

The validation of the mode decomposition is done for the surface-mounted cube by comparing to the modes computed by Manhardt & Wengle (1993) [13]. Since the same POD modes are obtained as in the reference case, it is assumed that DES solutions contain adequate velocity fluctuations to compute POD/DMD modes. Since the DMD is new within fluid mechanics, no reference case exists for comparison, relevant to this project. Instead the DMD modes are compared to POD modes, to verify that the DMD modes are computed correctly. The number of snapshots is found to be an important parameter for the decomposition modes. Therefore, a method to verify that adequate number of snapshots, is proposed and used for all flow cases.

In order to have reliable results two different techniques to investigate the convergence of the POD modes were proposed and tested. It was found that long sample times are needed to have converged POD modes and that the two convergence methods give consistent results. The converged modes were analyzed and three different groups of flow structures were characterized. The first group is simply the mean flow and the two others represent perturbations to this mean flow. They are dominant in different regions of the flow, the first represent perturbations at the shear layer and the second perturbations in the wake of the cube.

The method of using DES flow field with POD and DMD, which was validated (see [G]), was applied to the Aerodynamic Train Model. Strong similarities between the POD and DMD were found, both for the spatial modes and the temporal modes in Muld et al. 2010 [J]. The dominant flow structures were associated with the two counter rotating vortices in the wake.

The simulation on a full train geometry using DES is computationally very demanding. In order to reduce the computational cost in order to include the computations as early as possible during the design phase of a train, several approaches have been pursued. One is to assess the sensitivity of slipstream to the upstream flow. During the project, studies have been made of various techniques to simulate the wake flow on a small calculation domain with boundary data upstream conditions. In DES simulations, an efficient way to study the effect of the upstream flow conditions on the wake structures of a train is to consider a boundary value problem, where the upstream flow conditions are given as boundary data. The aim of the study was to get a quicker simulation technique based on a thorough knowledge on the sensitivity on different parameters in the upstream data, such as length and time scales in the turbulent quantities and resolution by the computational mesh and the time step at the computational boundary. The methods tested were everything from simple methods predefined stripe data from RANS calculations, to advanced methods called Recycling. The conclusion of this work was that it was not possible to use any of these methods in a simple way to reduce the computation domain for railway applications. For example, for recycling to be adequate, this approach should be implemented in a manner using technically advanced programming to have an opportunity to give good results. Paper [L] investigates the possibility of reducing the domain upstream of the separation and imposing a boundary condition somewhere along the train.

In order to minimize the computational effort involved, differences between Reynolds Averaged Navier Stokes (RANS) calculations which are also carried out in the industry and the advanced DES methodology that has been applied in this project has been studied in detail regarding slipstream. This has resulted in a Master thesis (see [I]) in which the flow around the ATM has been simulated, using both steady and unsteady RANS. A detailed grid study is performed and both the overall drag and velocity profiles in the wake are used to judge convergence. Nine different Reynolds numbers are simulated to investigate the influence on the drag and lift coefficients, ranging $4 \cdot 10^4$ to $1.11 \cdot 10^6$ (full scale). Both the drag and lift varied along the whole range of Re. By looking at the different contributions to drag, it is clear that the viscous drag decreases when increasing the Re and the pressure drag increases. The flow fields are also compared to results from previous computations using DES. It is found that the URANS computations does not include the same small scales as the DES, however the large fluctuating motions is described well by the URANS, for instance in term of frequency. The TSI velocities are extracted from the URANS computations and the value of $u_{2\sigma}$ agrees well with the DES results.

Impact of carbody width on slipstream evaluation following TSI

In order evaluate the CFD computations according to the TSI procedure, the reference frame has to be adapted from the train fixed reference frame in the CFD computations to the ground fixed reference frame in the TSI-measurements. In the CFD reference frame, the probe moves with the speed of the train. A method to extract the velocity in ground fixed probes was therefore proposed and tested. The velocity profiles were filtered with a 1s time average in accordance with the TSI regulation. The velocity profile showed a large scattering in both peak value and peak position between probes. As outlined previously, the formulation in the current TSI regarding slipstream is based on the experiences with trains compliant with the UIC profile. To investigate the effect of wide body trains, the mean streamwise velocities have been analyzed. A corrected TSI-position was introduced to obtain slipstream velocities at

the same distance from the train body. For the ATM, the corrected TSI-position is at the same distance from the carbody of the ATM as the distance of the TSI-position from the carbody of the CRH1 (1.33 m). Analogously, the corrected TSI-position for the CRH1 is located 1.49 m from the car body of the CRH1, which is the distance from the TSI to the ATM. The different distances are shown in Figure 5. It should be noted that the width considered are the maximum width of the car. By introducing a corrected TSI position, the effect of wide body cars is investigated. It is found that a wider version of a train creates larger slipstream velocities (for reference see [D] and [E]).

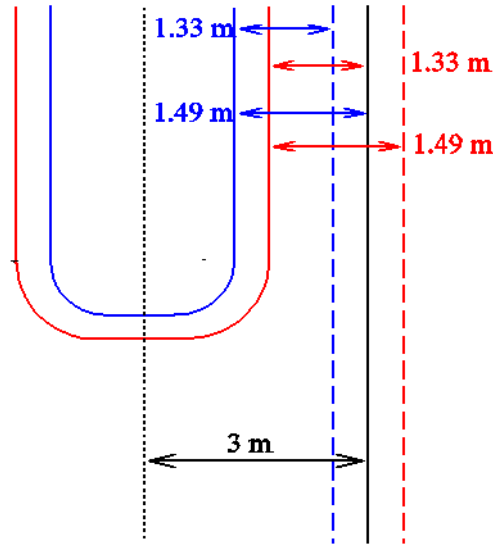


Figure 5: A schematic top view of the TSI and corrected TSI positions for the ATM (blue) and CRH1 (red).
 Solid colored lines: train surfaces, solid black line: TSI position, dotted black line: symmetry line, dashed colored lines: corrected TSI positions.

The TSI procedure is applied on the DES computations and 20 probes are extracted for the ATM. Both the instantaneous and time-filtered velocity is shown in Figure 6. A strong spread is apparent in the results between the different probes. For some samples the measured maximum velocity is low, but high slipstream velocities occur at some instances. The highest slipstream velocities are clearly located in the near wake region, which is consistent with the results in [23]. The measured values is $u_{2\sigma} / U_\infty = 0.154$ for TSI-platform and $u_{2\sigma} / U_\infty = 0.198$ for TSI-trackside, which corresponds to $u_{2\sigma} = [8.6 \ 11.0]$ m/s for a train at 200 kph. This is with margin under the threshold values (15.5 and 20 m/s) for the TSI.

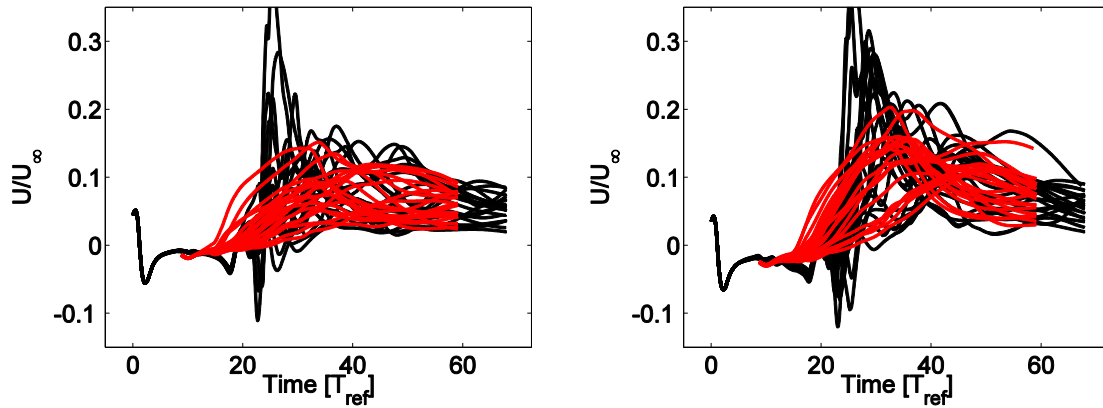


Figure 6: Time instantaneous (black) and time averaged (red) velocity in a ground fixed coordinate system for the ATM at $0.4d_h$ over the platform and $0.067d_h$ over TOR on the trackside. $t=0$ corresponds to when each probe passes the first measurement point.

The mean streamwise velocity in the TSI and the corrected TSI position for the platform TSI is shown in Figure 7. It is evident that as the measurement position is moved closer to the center of the track, the mean velocity close to the peak increases. This indicates that it is more challenging for wide body version of the same train to fulfill the TSI although it is very difficult to quantify this effect. It is likely that larger differences exist comparing different train types, meaning that a wide body train might not necessarily be worse than another train compliant to the UIC profile.

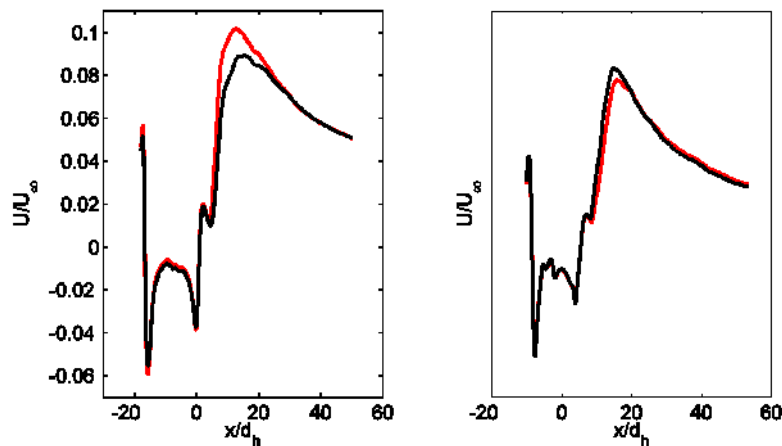


Figure 7: The mean velocity in the TSI-position (black) and corrected TSI-position (red) on the platform side for the ATM (left) and the CRH1 (right). The ordinate (y-axis) is omitted for the CRH1 due to the confidentiality of the train geometry. For the ATM, $x=0$ is at the beginning of the tail of the last car and for CRH1 at the middle of the tail car.

Impact of tail geometry on slipstream flow structures

In order to gain increased knowledge on the mechanisms governing the slipstream of a train, a major study on the impact of geometry of a train on its slipstream has been carried out within the project. In this study, the simulated flow behind two train geometries, CRH1 and ATM, has been examined in more

detail with respect to the flow structures. The two different geometries were chosen since the flow immediately behind the train is of a different type. However, the same structures are dominating further behind the train. One of the conclusions of this work is that the structures in the wake which are similar for the two geometries are the dominant ones for slipstream. To make this conclusion mode decomposition was crucial. The results have been presented in [D].

In the literature, two flow topologies were found in wake of different bluff bodies (see [2],[14],[24]), a quasi-steady separation bubble and two counter-rotating vortices. These two flow topologies have also been identified in the wake behind the ATM and the CRH1. By investigating the streamlines, the q -criterion, the mean flow and the mean pressure coefficient at the slanted back surfaces, it was found that the flow topologies are different for the two flows. The flow behind the CRH1 separates by forming a separation bubble, while behind the ATM the flow forms two counter-rotating vortices. The two different flow topologies can be visualized in many different ways, in Figure 8 this is done by plotting the streamlines of the time instantaneous flow. For the ATM, the flow from the top stays attached as it passes over the slanted back surface. This causes the pressure to decrease and the streamline from the side is sucked towards the center. As the flow from the sides separates over the side edges it curls into *counter-rotating vortices*. For the CRH1, the flow from the top and sides separates from the back surface, creating a *separation bubble*, which can be seen as the low velocity streamlines adjacent to the slanted back surface. It should be noted that this is the characterization of the separation of the flow. The flow behind the CRH1 still contains counter-rotating vortices, which are formed around/behind the separation bubble. An estimation of the angle of the back surface is approximately 50 degrees for the ATM and 33 degrees for the CRH1. This could be compared to the critical angles found (see [2],[14]), which are around 47 and 60 degrees, respectively.

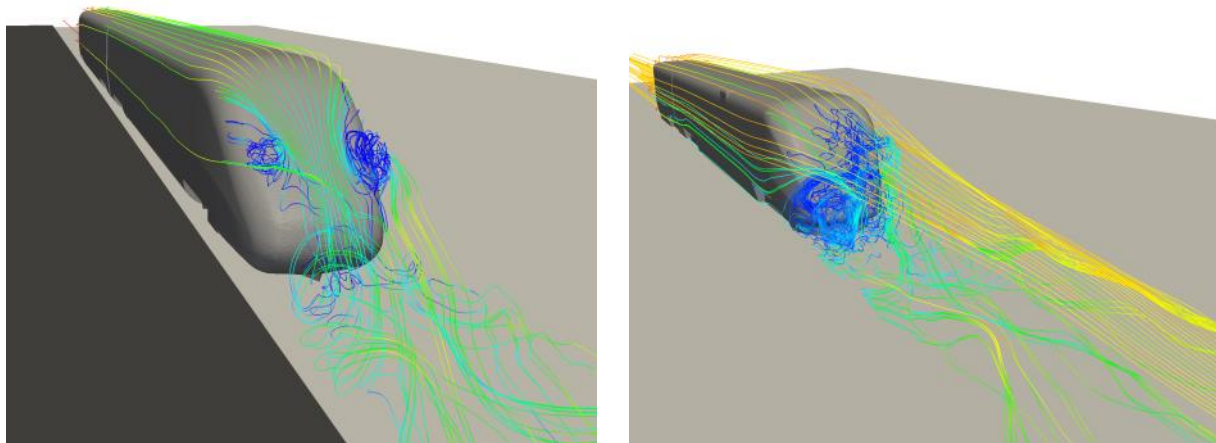


Figure 8: Streamlines of instantaneous flow colored by the speed of the flow around the ATM and the CRH1.

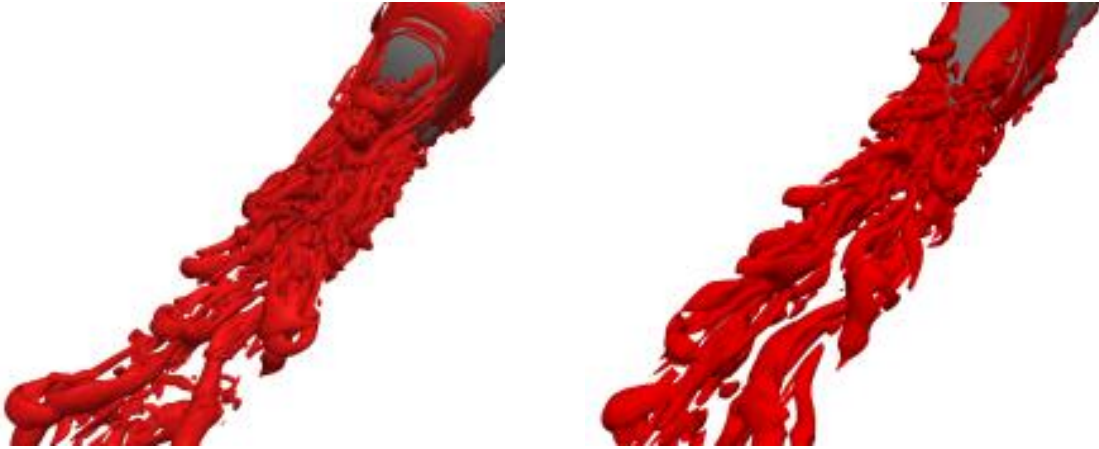


Figure 9: Isosurface of instantaneous Q-criterion ($Q=2$) in the wake of the ATM (left) and CRH1 (right)

Despite the difference in flow topology the dominant flow structure, identified by reconstructing the flow field, is vortex shedding for both train geometries. (for reference see [D],[E]). It is difficult to determine which flow structure each mode represents only by looking at isosurfaces of the spatial part. Instead, taking the mean flow and the first fluctuating mode couple shows how this mode couple affects the mean flow, first taking the ATM as an example and then looking at the CRH1.

Reconstruction of the flow field associated with the first fluctuating mode couple has been performed on the ATM, and three snapshots of the flow are shown in Figure 10. The snapshots show the time evolution of approximately half a time period. This flow structure affects the counter-rotating vortices, which is the dominant part of the mean flow, by making one of them stronger and the other one weaker at a certain streamwise position. At a later time this structure has moved downstream and now the other vortex is stronger at this position and the first one is weak. This flow structure is hence identified as vortex shedding.

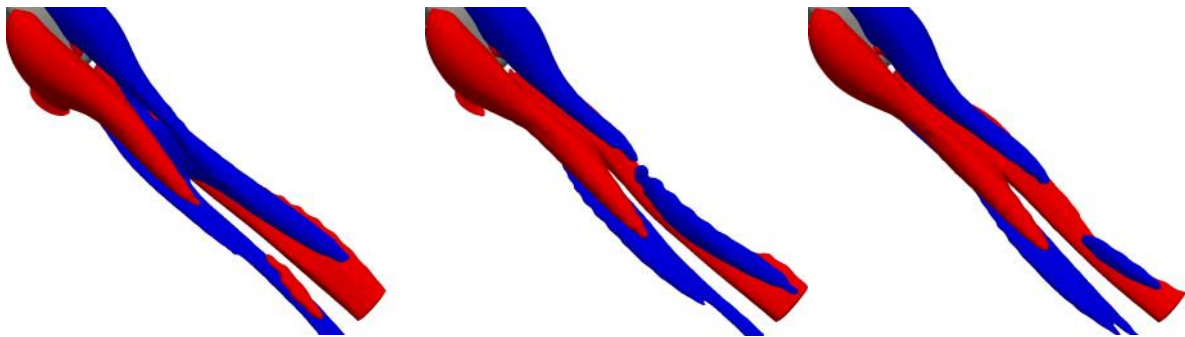


Figure 10: The reconstructed flow field from POD modes 1,2 and 3 on the ATM at three different time instances. Isosurfaces show positive and negative spanwise velocity (v).

The same reconstruction of the flow field associated with the first fluctuating mode has been performed on the CRH1, and three snapshots are shown in Figure 11. In this case, the snapshots span around 70% of a time period. The same type of motion as for the ATM is also found for the CRH1, which is oscillating strengths of the counter-rotating vortices from one side to the other. This means that even though the

flow topology is different, the most energetic flow structure behind both the CRH1 and ATM is vortex shedding.

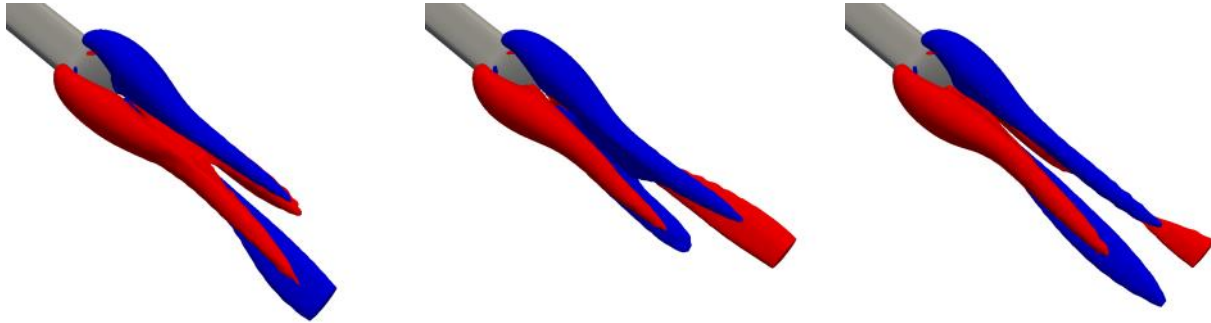


Figure 11: The reconstructed flow field from POD modes 1, 2 and 3 on the CRH1 at three different time instances. Isosurfaces show positive and negative spanwise velocity (v).

An interesting flow structure that was found behind the CRH1, but not the ATM, is the low frequency motion associated with mode 6. This mode is singular, it is not found in a pair of modes, and therefore the reconstruction has been performed using only two POD modes. Three snapshots of the zero isosurface of streamwise velocity are shown in Figure 12. The zero isosurface shows the region of recirculation, i.e. the separation bubble. At different time instances the size of the separation bubble changes size, moving inwards and outwards. This is the only among the first eight modes that are directly associated with the separation bubble and not the counter rotating vortices. This motion is very slow, much slower than the vortex shedding.

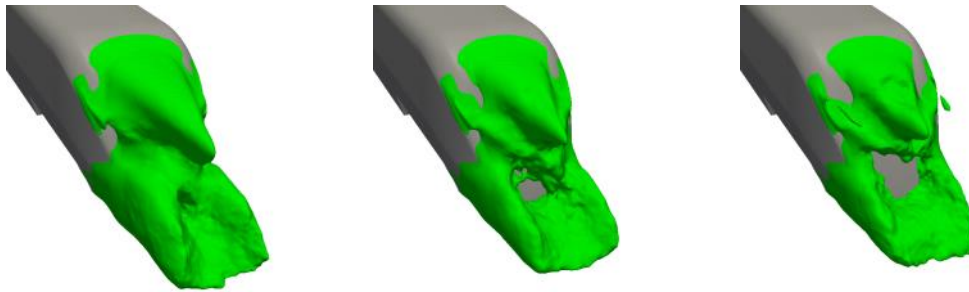


Figure 12: The reconstructed flow field from POD modes 1 and 6 on the CRH1 at three different time instances. Isosurface show zero streamwise velocity (u).

To gain further inside in the temporal evolution, it is of interest to investigate which DMD modes have a large influence on the TSI velocity in order to understand which flow structures that are the dominant ones in the slipstream. This is done by looking at the contribution of each mode at the TSI measurement position. For each mode, 20 time samples are created by randomly choosing an initial phase and traversing a probe through the domain in the same manner as described above in the section above. The TSI procedure is then applied. Due to the small size of the DMD domain, a complete 1s time average cannot be applied. The mean filtered velocity for each mode is plotted as a function of frequency in

Figure 13 for the ATM and the CRH1. It is not exactly the same mode that is dominant in energy that is most important for slipstream, but both of them are in the same frequency interval. The frequencies of the most dominant flow structures are investigated in the next section. The most dominant modes for frequency and energy have approximately the same flow structure. This flow structures is vortex shedding. It is interesting to note that there are a few peaks in the range of frequencies that are excited by POD mode 4, and since multiple DMD built up this POD mode all the contribution must be taken into account, which could give a large contribution.

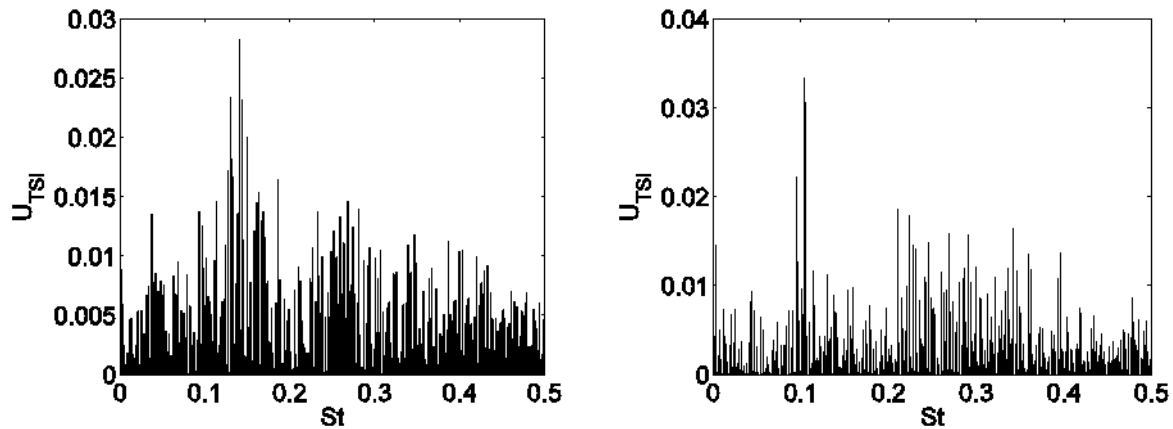


Figure 13: The TSI-velocity for each DMD mode for the ATM (left) and CRH1 (right).

Comparing flow structures from POD and DMD

In order to gain a deeper understanding of each set of modes, an ambitious work has been performed to compare the two different decomposition methods, POD and DMD. The conclusion from this work is that the decomposition into modes is a very useful method to analyze the flow in comparison with the study of flow directly without decomposing into nodes. POD is seen to be computationally more robust method but the advantage is that modern DMD when given per frequency, which could be an advantage for application of flow control. The work is reported in [C] and [J].

The two decomposition methods have been compared in this project for all different geometries considered. The general conclusion is that the same flow structures are extracted with both methods however the relative importance of a flow structure might be different for POD and DMD. This is since a flow structure could be described by a single mode for one of the decomposition methods, while for the other decomposition method the energy is divided among multiple modes.

Looking at the spatial parts, POD and DMD modes show many similarities, despite the different formulation of the methods. As an example a selection of the dominant modes in the wake of the CRH1 is shown in Figure 14. Mode 1 should be equal, since for correctly computed modes, both POD mode 1 and DMD mode 1 correspond to the mean flow. POD mode 2 is very similar to DMD mode 2, in terms of size and position of the structures, it is only the phase of the motion that is changed. POD mode 4 has similarities with DMD mode 6, however the connection is not as clear as for POD mode 2. POD mode 4 seems to be built up by the structure in DMD mode 6 plus some additional motion. Last, POD mode 6 is

similar to DMD mode 3. In this case the relative importance has changed between POD and DMD, i.e. POD mode 4 has higher energy than POD mode 6, but DMD mode 3 has higher than DMD mode 6. This could be because the energy content in POD mode 3 is divided on multiple DMD modes, 6 being one of them. Looking at the temporal part in the next section, the connection between the POD and DMD modes becomes more clear.

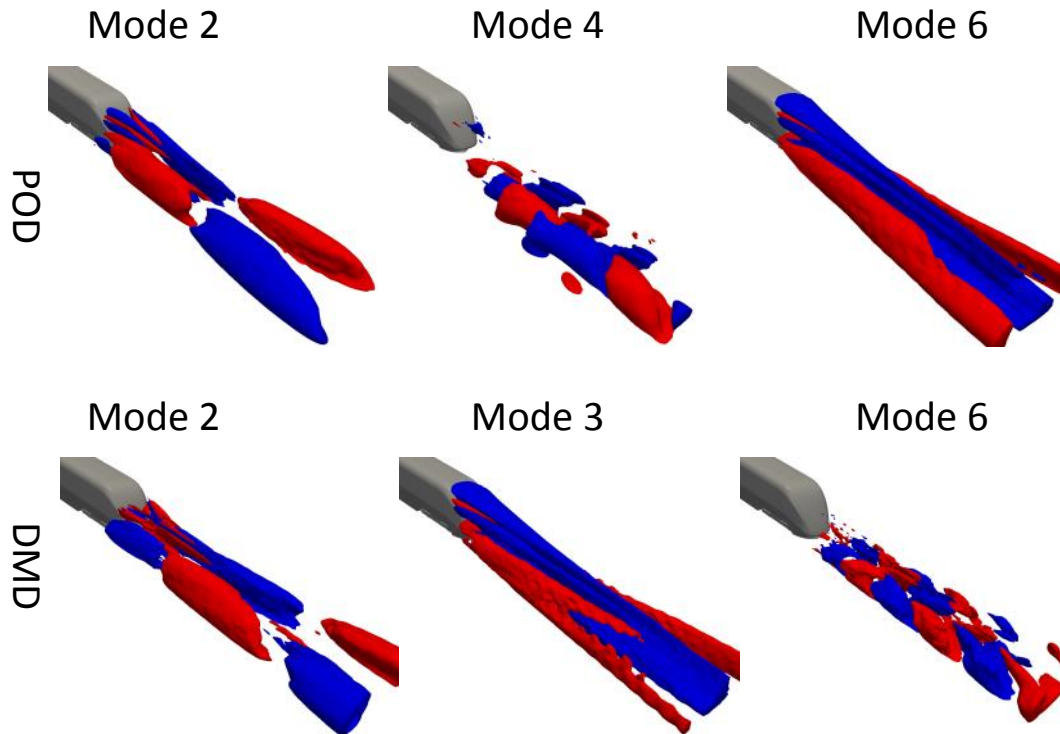


Figure 14: Isosurfaces of positive and negative streamwise velocity (u) for a selection of POD and DMD modes of the CRH1, red positive, blue negative. The flow is coming from top left going down right.

Comparisons between POD and DMD are also done in the larger domain (B) around the surface-mounted cube, which is shown in Figure 15. Here, POD mode 2 resembles DMD mode 10, POD mode 5 corresponds to DMD mode 2 and POD mode 8 to POD mode 13. Also in this case, a relative change occurs in importance between the structures in the modes. It is also evident that the POD modes are smoother than then DMD modes.

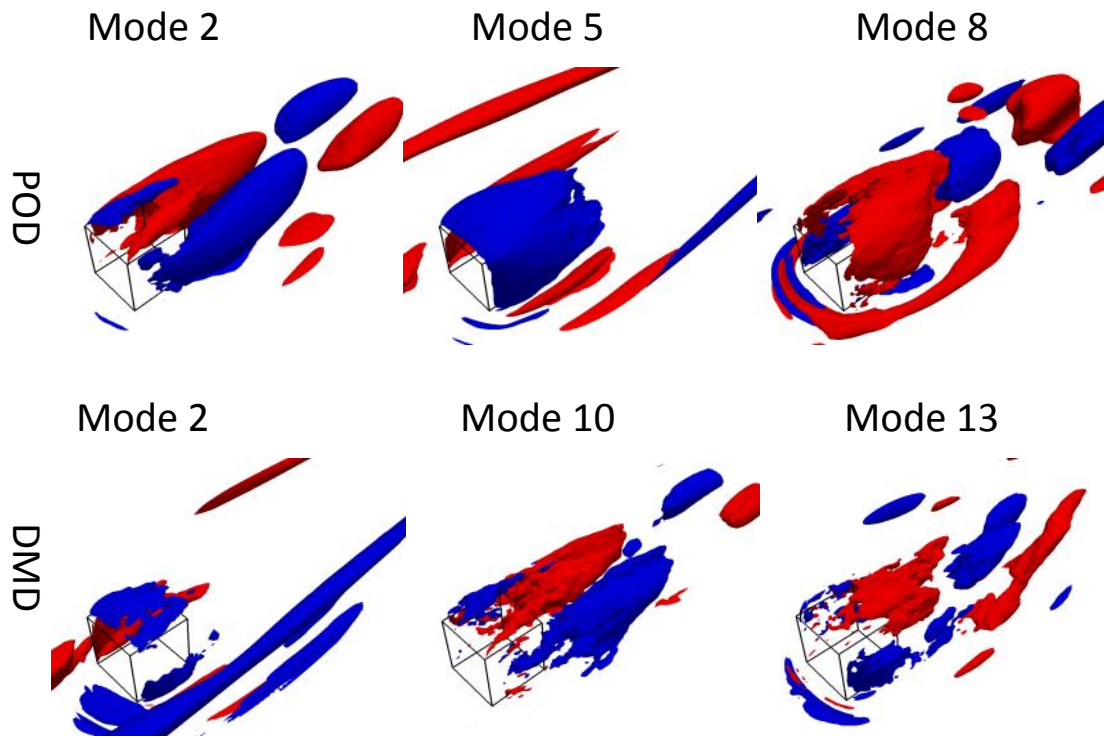


Figure 15: Isosurfaces of positive and negative streamwise velocity (u) for a selection of POD and DMD modes for the larger domain on the surface-mounted cube, red positive, blue negative. The flow is coming from bottom left going up right.

The time evolution of the POD modes is governed by arbitrary functions whereas for DMD modes each mode corresponds to a single frequency. In order to compare, the frequencies of the POD mode coefficients are investigated. This is done by taking the Fourier transform of the mode coefficients of each POD mode. The amplitudes of the Fourier transform show which frequencies dominate the mode coefficients of each mode. The amplitudes for POD modes 2, 3 and 4 on the CRH1 are compared to all the DMD modes, as function of frequency for each DMD mode, in Figure 16.

For all cases considered, it is found that a peak in the amplitude of the Fourier transform also is represented by a DMD mode with high magnitude of the Ritz vector. For some POD modes, often the first fluctuating mode, the frequency spectrum has a narrow peak, meaning that the arbitrary function is oscillating at almost one single frequency. In these cases it is found that the spatial DMD and POD modes are very similar, implying that the dominant flow structure extracted by both methods is the same. In other cases the POD frequency spectrum is broader. In these cases, the spatial part of the POD modes share similarities with multiple DMD modes in the range where peak in the frequency spectrum occurs.

The mode decomposition performed in Paper 2 was extended and the extracted flow structures were analyzed by reconstructing the flow field with a subset of modes (see [C]). The reconstruction was found to be an intelligent way to visualize the flow structure. The dominant flow structure was found to be vortex shedding, as mentioned above. The second flow structure was found to be bending of the counter-rotating vortices. The method to investigate the convergence of the POD modes was modified

in order to be extended to DMD modes. The largest modification is that the complex magnitude of the DMD modes was used, since a phase-shift was found between DMD modes computed with different amount of snapshots.

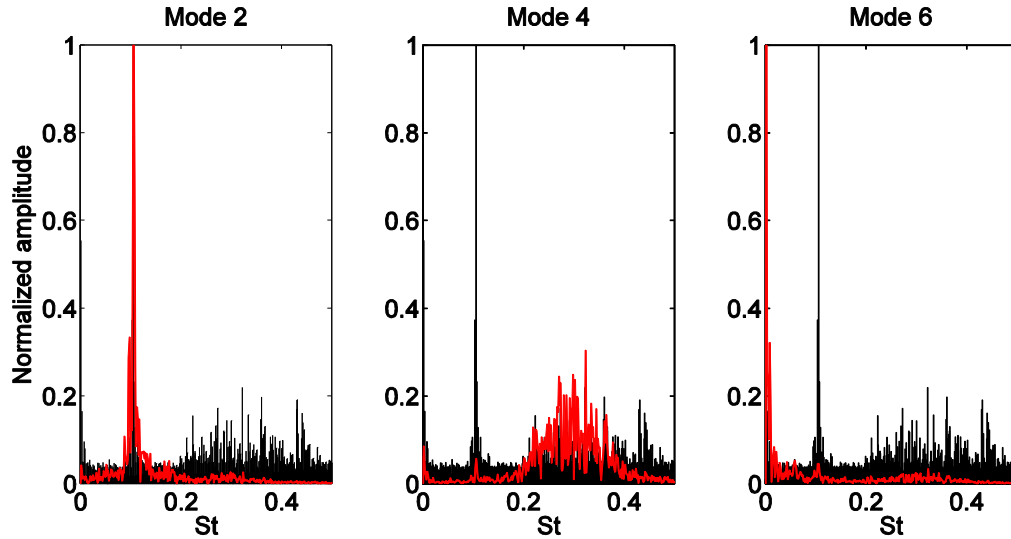


Figure 16: Normalized spectrum of Fourier transform of the POD mode coefficients for modes 2,4,6 (red) compared with the normalized energy for each DMD mode as a function of frequencies (black), for the CRH1

Impact of train length on wake flow pattern

Due to the long slender body of a train, the size of the boundary layer at the end of a long train is of the same order of magnitude as train width. A detailed analysis of different wake structures with regard to the boundary layer thickness at the last car prior to separation based on the different decomposition methods, POD and DMD, has been performed. Especially flow cases with thick boundary layers have been studied. Thick boundary layers correspond to long trains with a large number of cars. Within the project, studies of the effects of the length of the train on the slipstream have been performed. The effect of the size of the boundary layer on the wake flow structure is investigated by simulating the flow around the ATM train with different lengths. Large-scale calculations of train sets with two, three and four wagons of the ATM geometry have been conducted and the results analyzed with POD and DMD mode decomposition showing that the size of the boundary layer at the point of separation influences the wake flow patterns. The conclusion of this work on the impact of the train length on the slipstream is that generally trains of different length exhibit the same structures in a wake, but the frequency of the vortex shedding that occurs in a wake changes. The results were compared to experimental studies of flow behind a flat plate, and the results are consistent. To our knowledge, this is the first time that this effect is studied for such a complex geometry as a train. The work was published (see [F]).

In this paper, wake flow of three different configurations of the ATM (with 2, 3 and 4 cars) were simulated in order to investigate the effect of momentum thickness on the wake flow structures, for an applied 3-dimensional geometry. Using empirical formulas, these configurations of the ATM could be shown to correspond to trains in full scale with 6, 9 and 12 cars traveling at 200 kph. The momentum thickness is used to compare the size of the boundary layer at the last cars of the train. An empirical

formula of the momentum thickness as a function of downstream position x is given for a flat plate by Munson et al. (2002) (see [15]) which can be used to estimate the difference in momentum thickness between a full scale train at full speed and the scaled model at reduced Reynolds number used. The momentum thickness as a function of streamwise position was extracted from the simulation for all configurations and compared to the empirical formula for a flat plate boundary layer. The empirical formula agreed well at the front of the train, whereas further downstream, the effect of the curved surface, inter car gaps and the tail is believed to alter the profile. The flow topology was found to be the same for all three configurations. The change in size of the boundary layer does not alter the flow topology, the flow structures remain the same. The dominant flow structure was the same, which is vortex shedding. However, the wave length and frequency of the vortex shedding was different. The vortex shedding frequency was found to decrease as the momentum thickness increases in front of separation.

The streamwise component of the first POD modes for the three different configurations of the ATM is shown in Figure 17. The mean flow is visually the same and hence the topology of the flow is the same. Even the first fluctuating mode couple looks very similar for the different configurations, with the exception of the wave lengths. For the shorter train the structures are shorter and for the longer train the structures are longer. In Paper 5, it is also verified that the reconstructed flow field of the first fluctuating POD mode couple exhibit the same characteristics for all configurations.

For all the configurations, a frequency is dominant in the spectrums of the POD and DMD modes. The dominant frequency is plotted versus the momentum thickness in Figure 18. It is evident that the Strouhal number decreases as the momentum thickness and length of the train increase, which is consistent with the results found by Rowe (2000) (see [16]).

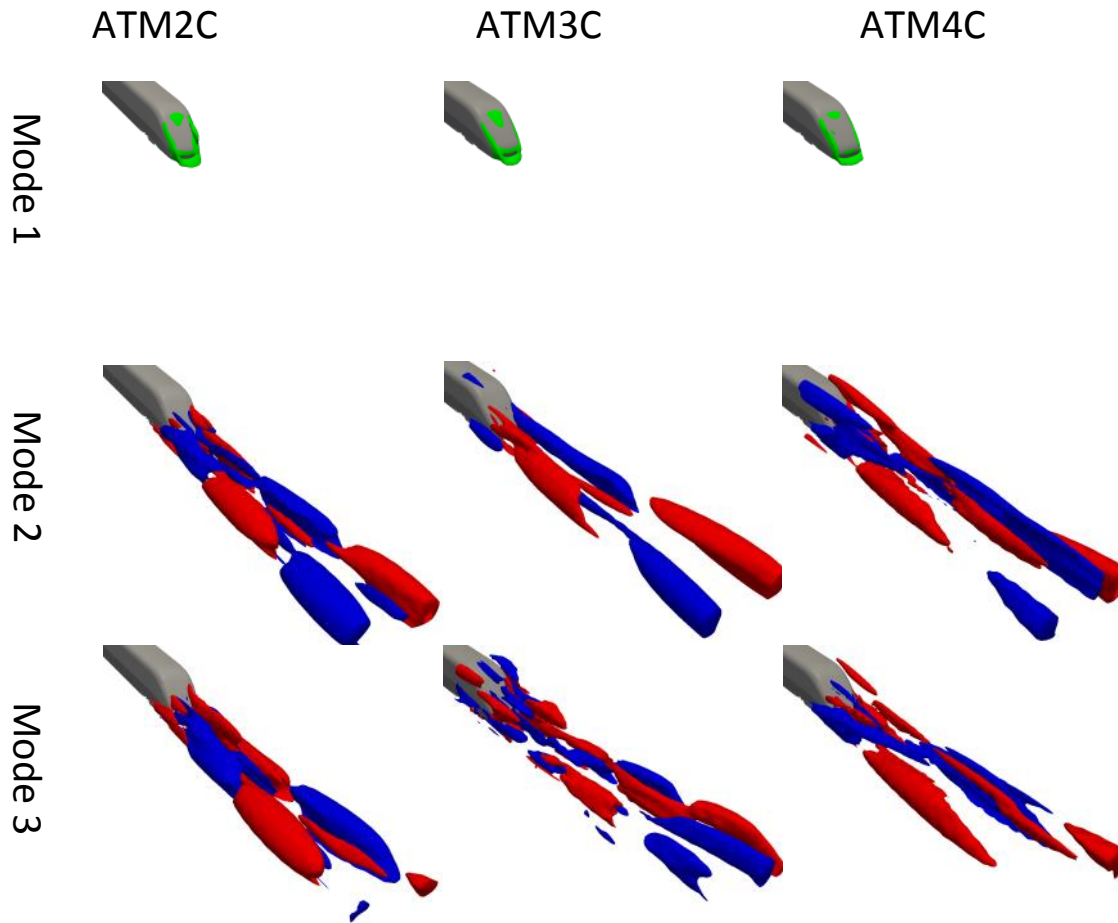


Figure 17: Isosurfaces of positive and negative streamwise velocity (u) for the first three spatial POD modes of the three configurations of the ATM, red positive, blue negative, green zero. The flow is coming from top left going down right.

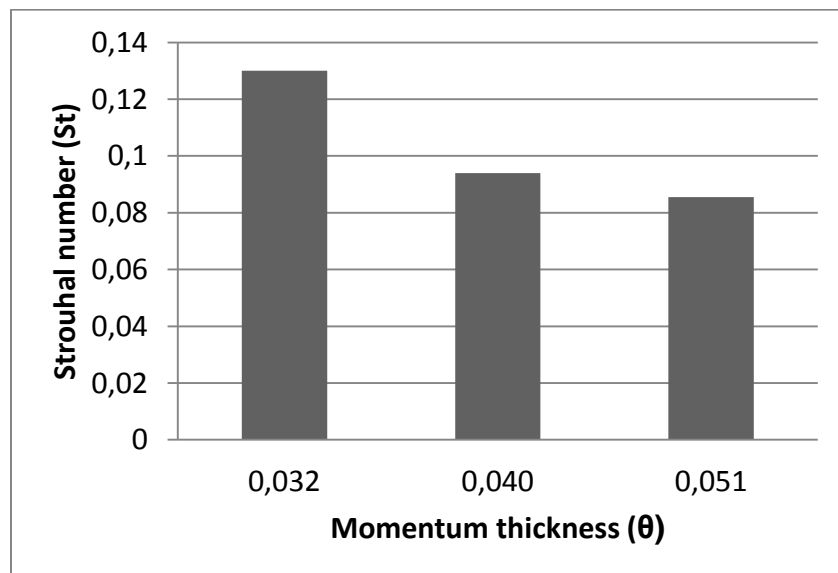


Figure 18: Strouhal number of the most dominant structure in the wake as a function of momentum thickness at the train body close to the tail.

5. Aerodynamic optimization

A comprehensive and innovative optimization process has been developed during the course of the project which helps to develop and build new products by calculating the best way to reduce aerodynamics drag and to fulfill the requirements regarding head pressure pulse, slipstream velocities and safety with respect to cross-wind. The system is based on genetic algorithms that use parameterized, three-dimensional models, detailed simulation of aerodynamics quantities in question and a decisive optimization software.

Designing the outer shape of a train has major impact on the aerodynamic performance of the vehicle. The goal was to generate a design which has a good performance both with respect to slipstream, drag and head pressure pulse since the front for most modern trains may well operate as the rear as well. The overall goal of aerodynamic optimization for high speed trains is to design a train which is as efficient as possible. In particular the objectives for the work presented here are the reduction of aerodynamic drag and the increase of stability with respect to cross-wind. Reduction of aerodynamic drag saves energy demand of trains and reduces costs. Limiting drag and maximizing stability also increase acceleration, which reduces traveling time. Stability with respect to strong cross-winds is a safety requirement. The objective is to give input to front design including shape constraints. This includes the front design considerations such as space envelope, crash structure, ergonomic constraints such as the visibility of signals at the track and the space available for the passenger compartment. These geometrical constraints have been partly implemented as simple bounds of the parameters and partly as constraints in the current approach.

All the above-mentioned phenomena need to be taken into full consideration in the design stage of a new train. If the train fails to meet one or more criteria in the verification testing process, this will likely cause serious delays and high additional costs, as many aerodynamic phenomena are dependent on the trains outer shape which is frozen at an early stage in the design process. Also, the interdependence between all the above-mentioned phenomena should be studied by varying parameters systematically. Also for optimization of aerodynamic performance a systematic parameter variation is crucial.

Traditionally, a way of exploring the set of design modifications with regard to their aerodynamic performance has been to check them experimentally in the wind tunnel. Here the iterative development of further designs is based on theory and engineering skills. However, this approach is rather costly and time consuming. Further, in many cases due to the large number of possible designs it is unlikely that the truly optimal design in the sense of Pareto can be found without assistance of automatic tools. Implementing the approach of automated optimization in train aerodynamics the target is to overcome several disadvantages of the common design process. On the one hand the conventional iteration between designing and evaluating the model is speeded up and directed by an optimization algorithm. On the other hand the aim is not only to fulfil all given constraints and requirements but to deliver the optimal solution. The increasing performance and price drop of today's computers facilitate the use of modern CAE based optimization tools for determining the optimal parameters for the external shape of trains.

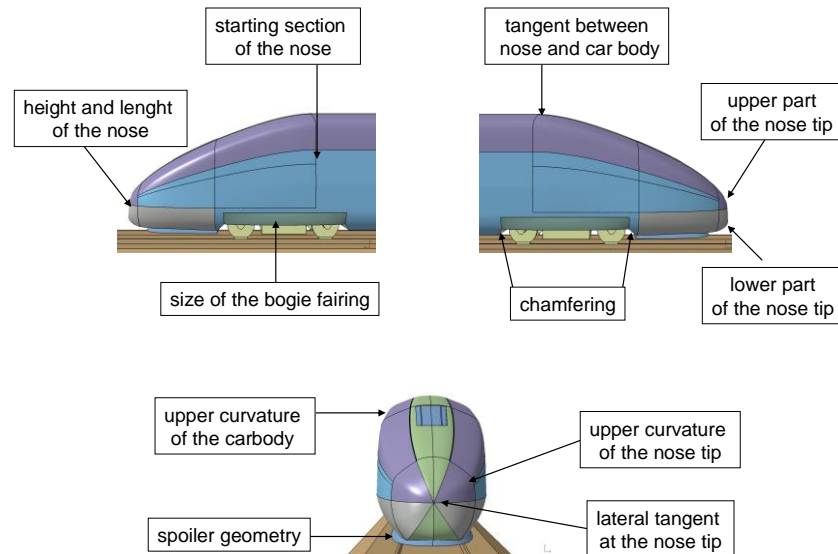
With this approach, a mathematical optimization algorithm such as the Simplex algorithm, gradient-based methods or genetic algorithms can be utilized for the optimization of the shape design. This requires the optimization problem to be defined with an objective function which includes the costs of the design that one wants to minimize using design variables. The conditions which have to be satisfied are introduced as constraints. This includes the front design considerations such as space envelope, crash structure, ergonomic constraints such as the visibility of signals at the track and the space available for the passenger compartment as well as economical aspects. In order to fully exploit the possibilities of this approach a fully automatic loop including the generation of candidate shapes based on a parameterized geometry, the preparation and generation of a computational mesh and the evaluation of the design is required. In process developed, the commercial software ModeFrontier has been utilized as process integrator and provides the optimization algorithms. For the single objective optimization the simplex algorithm and genetic algorithms have been used.

A typical setup for an optimization process focusing on an aerodynamic problem includes the creation and configuration of the parameterized geometry, the generation of the mesh for calculation, the calculation and computation of the relevant variables and the computation of an optimized parameter setting using an optimization algorithm. Note that all components have to be set up so they can be integrated into one process flow automatically without manual manipulation. It has to be kept in mind that the stability with which the different components perform has significant impact on the outcome of the optimization as the major part of the designs have to be evaluated in the correct way in order for the optimization algorithm to converge towards the true minimum. A distinct feature of any aerodynamic design process is that it is computationally costly and particularly time consuming if the number of degrees of freedom is high. Therefore a reliable and efficient tool is needed in order to determine which design under the current conditions is suited best.

One challenge is to organize all tasks in a manner so that they can be integrated into one optimization loop without requiring manual input. Prior to this project, the process of preparing a simulation included a lot of manual manipulation starting with the preparation of the model for CFD applications in CATIA, the mesh generation process and the simulation including pre- and post-processing. Furthermore the whole complexity of designing a train is to be considered in the loop of optimization including ergonomic requirements for integrating the drivers cab, crash structure concept and integration, ergonomic constraints on the visibility of signals at the track taking into account sitting and/or standing drivers, bogie movements and aspects regarding the industrial design of the vehicle.

The implementation was deduced from a general approach for shape optimization on the base of a parameterized model. Automated shape optimization requires a parameterized model, which is manipulated by altering the design variables until the optimal set of geometry defining parameters are found. Therefore the model is evaluated in a CFD simulation and the generated data together with the current parameter setting enable the optimization algorithm to calculate an improved parameter set for the next iteration. All design variables and their ranges are initially defined within ModeFrontier and only the current setting is then applied to the CAD-model through a direct interface. The resulting CAD model is transferred via a SSH connection to a workstation or cluster, where batch scripts call the respective tools to prepare the mesh for the simulation. After the simulation the outputs are transferred

back to ModeFrontier, which evaluates the final target function in Matlab and assigns the values to internal output variables. This information together with the current parameter setting is fed back to the optimizer, which generates, by means of the collected data, a new improved parameter setting for the following iteration. ModeFrontier manages the whole file system generated during the optimization, which is very useful for handing over data from one tool to another as well as for error tracing.



Generating the parametric CAD model and defining the range of the parameters is one of the most sensitive parts in the process of optimization. The goal is to generate a model that gives a high degree of freedom to the optimizer, keeps all the necessary constraints by minimizing the amount of parameters at the same time. The objective is to give input to front design including shape constraints. This includes the front design considerations such as crash structure, industrial design and ergonomic constraints such as the visibility of signals at the track and the space available for the passenger compartment. A parameterized model should be capable to reproduce all important features like different fronts, spoilers, pantographs, bogie cut out and cross sections, while a-priori integrating most of the requirements mentioned above. Additional constraints like the maximal extensions of the shape are met during the optimization by restricting the parameters respectively. The parameterization has high impact on the outcome of the optimization. An optimization is only capable to identify the best design with respect to the parameterization. Therefore, it is important that the parameterization captures all relevant features with regard to the optimization problem. It then offers a choice of the best possible solutions to optimize the vehicle's aerodynamic performance. However, the number of parameters should be as small as possible to keep the computational effort in affordable limits. To enable the optimizer to find such a solution several geometrical features of the head/tail (see picture above) were parameterized. Changing those features enables to generate a huge variety of different shapes of completely different aerodynamic quality defining a powerful basis for the optimization.

Modifications of the external shape pertain to the shape of the front up to the first bogie keeping the cross sectional area at the connection to the first car constant. The parameterization has been carried out in CATIA. The focus of this optimization was on the shape of the head/tail of the train but the bogie cut outs and the curvature of the carbody are parameterized as well. In the bogie region a parametric bogie cut out was implemented that could be varied in length and by applying a variable chamfering at its boundary. The chamfering interacts with the variable fairing that covers the not chamfered part of the cut outs.

However, it has to be kept in mind that the term “best design” is relative and highly depending on the parameterization. The model was first developed to be suited for single objective optimization. In order to be suitable for multiobjective optimization, the model had to be revisited due to the increased number of freedom and therefore fast increasing computational effort in a multiobjective optimization. The parametrized model had to be adjusted for that purpose. The updated parameterized model allows examining both trains compliant with UIC and Scandinavian gaging in the same model.

With this approach, a mathematical optimization algorithm such as the Simplex algorithm, gradient-based methods or genetic algorithms can be utilized for the optimization of the shape design. The optimizer used is ModeFrontier which provides a variety of different algorithms for direct optimization and for design of environment (DOE) applications as well as means for evaluating and post processing the generated data. The optimization algorithms provided in ModeFrontier have been implemented by the company ESTECO which is distributing the software.

For the optimization both the simplex algorithm and genetic algorithms have been used. The two optimizers chosen during the course of the project are the Simplex algorithm, following the approach by Nelder & Mead [2] and the genetic algorithm MOGA-II [3]. The version available for the simplex in ModeFrontier has been updated in order to be applicable also for discrete variables and constraints. In the following the description of the algorithm according to the documentation in ModeFrontier is given. SIMPLEX is a sequential algorithm for single objective optimization and cannot be parallelized. Suited for multiobjective optimization is a genetic algorithm based on principles derived for the explanation of genetic processes in nature such as selection, mutation and cross-over and applies them formulating an algorithm for optimization problems. The optimization algorithm used was the generic algorithm MOGA-2, which computes new designs generation by generation. Each member of a new generation is derived from its direct ancestors by randomly mutating and crossing over their genomes, in terms of their defining design variables. In the case that the successor is not worse regarding all objective functions replaces its parent, the natural procedure of selection. Genetic algorithms can also be used for single-objective optimizations. The advantage compared to the SIMPLEX algorithm is that they are not likely to get trapped in a local optimum since due to the genetic nature, a larger part of the design space is checked and alternative solutions with comparable performance are found. SIMPLEX advantage is on the other hand the fast convergence.

As a pilot project for this approach, an optimization of the shape with respect to one single objective function has been performed. The objective function is evaluated with respect to head pressure pulse. The objective function to be minimized during the optimization loop is the amplitude of the head pressure pulse. The evaluation is according to the specification in the TSI in which also the

measurement positions are specified and the maximum amplitude of the head pressure pulse is limited. The objective function is the maximum of head pressure pulse amplitude $max \Delta c_p$ measured at the 7 measurement positions which has to be lower or equal the maximum amplitude specified in the TSI.

The challenge for shape optimization involving aerodynamic computations is to resolve the structures which are significant in order to capture the trends. In order to develop an efficient method, two optimization loops have been implemented. One evaluates the objective function based on the solution for the inviscid flow at low computational cost using a panel solver. For higher accuracy the second loop evaluating the objective function based on a RANS calculation at the cost of moderate computational effort has been created using the polyhedral mesher in STAR-CCM+ and the RANS computation in STAR-CCM+.

Both parametric models are controlled using exactly the same parameters. The model for the use with the inviscid solver START contains less details as flow separation cannot be predicted well with such a method. Therefore the bogie cutouts have been closed, the bumpers have been excluded and the cutout for the coupler has been closed. Apart from that, both models are the same. For the computation in both START and STAR-CCM+, a grid resolution study has been carried out.

For the optimization loop using STAR-CCM+, polyhedral meshing methodology with prism layers to increase the resolution close to the walls has been applied. In order to model the turbulence, a k-epsilon turbulence model in a high-Reynolds number formulation has been used. The model has been chosen due to the higher robustness compared to e.g. a hybrid formulation for the wall model. The advective terms in the governing equations as well as the corresponding parts in the equations for the turbulence modeling are approximated using second order upwind-differences. A half plane of a one car model with a symmetry boundary condition has been computed in order to reduce the computational effort for the computation with respect to head pressure pulse. Since the track bed has significant impact for the correct computation of the head pressure pulse, the track bed according to TSI has been included.

For evaluation of the performance regarding cross-wind, the respective aerodynamic coefficients, computed in a RANS simulation in STAR CCM+, are passed over to a quasi static multi body simulation tool which models the train with two bogies, two wheel sets and the car body. This system features in total twelve degrees of freedom and is able to capture the displacements between the car body and the bogies (secondary suspension) and between the bogies and the wheel sets (primary suspension). Due to the displacements in the suspension the restoring moment is reduced and cross-wind stability decreases. The model incorporates the most relevant characteristics of cross-wind stability and is used during concept phase. The approach is quasi static, i.e. transient phenomena are not accounted for. The results nevertheless agree well with transient multi-body simulations which also capture track irregularities and are used for ride comfort analyses.

As mentioned at the beginning it is necessary to design the head and the tail equally. Since the optimal shapes of head and tail investigated separately are different it is a very challenging task to find a compromise that works well in both cases. Before setting up the multi-objective optimization the different objectives were investigated and optimized separately both to estimate the potential and to check possible correlations. Comparing the best designs, coming from the drag and from the crosswind

optimization confirmed that the two objectives are not correlated. Good performance in drag does not mean a good crosswind behavior, and vice versa. Maximising the load on the most critical bogie related to derailment has been chosen to be the goal for increasing the cross-wind stability. The behaviour of a train under cross-wind is a function of the angle of attack of the accumulated cross wind and air stream. Since it is too expensive to compute the so called characteristic wind curve in full, only one but characteristic point of the curve was taken.

A multiobjective optimization is necessary was therefore necessary. That means in first terms a doubling of computational costs for every iteration and a significant rise of the amount of iterations, mainly due to the fact that the dimension of the response spaces is enlarged and that straight forward algorithms like all gradient based and the SIMPLEX are not applicable. Furthermore a multiobjective optimization does not have a unique optimal solution as a result but with a set of Pareto optimal solutions. Optimality for a design in the sense of the Pareto means that it is not dominated by a design performing better in all objectives of the optimization.

This way, the process for aerodynamic optimization has been established during the course of the project. All constraints on a realistic train have been taken into account. Single objective optimization of the outer shape with regard to head pressure pulse as well as an optimization with regard to drag, slipstream and cross-wind has been carried out. The process enables close cooperation within different departments involved in the design of the outer shape. This way, significant aerodynamic features are incorporated in the whole process of planning and production. The compatibility of the new front design with the slipstream criteria was checked using wind tunnel measurements and is presented in the next chapter.

6. New improved front end design

The new improved front end design was created with the objective to fulfill the requirements regarding slipstream while keeping or lowering the drag aiming at lowering the energy consumption. Together with the findings from the multi objective optimization with regard to drag, crosswind and head pressure pulse and improved front design was developed.

The numerical studies regarding the slipstream performance on both the CRH1 and the new improved front end design were performed at KTH with the methodology described in an earlier section. The trains were simulated by solving the incompressible Navier-Stokes equations using the commercial solver StarCD v.4. The turbulence was modelled using Detached Eddy Simulation. The grids contained 28 million cells and 32 million cells for the CRH1 and new optimized train model, respectively. The simulations were in both cases carried out at a Reynolds number of 60.000 based on hydraulic diameter and free stream velocity. In the numerical simulation the ground is moving relative to the train, in the same manner as the full scale case.

The geometry has been tested in a wind tunnel in order to assess the slipstream performance experimentally. The measurement campaign was performed in the GroWiKa wind tunnel of the TU-Berlin, "Hermann-Föttinger-Institut für Strömungsmechanik". In order to assess the slipstream performance, a 1:25 scale train model with the optimized head design here trailing as the rear was used for the measurements. The flow field was measured using Particle Image Velocimetry (PIV), a 12-hole omniprobe, scanivalve probes and paint visualization.

The train model has been optimized for aerodynamic drag while ensuring that the requirements regarding crosswind stability and head pressure pulse were fulfilled at the same time and this test campaign aimed at investigating the influence of this optimization on the slipstream performance. The flow around the CRH1 train model was measured in an earlier measurement campaign using Laser-Doppler-Anemometry (LDA) and these results will be used for comparison with the train model.

The objectives of the wind tunnel campaign were to assess the slipstream performance of the optimized front design relative to the CRH1, to compare measurement data with CFD computations and to measure the slipstream and wake velocities with two different boundary layers at rear in order to mimic the effect of different train length.

The measurements were performed on a 1:25 scale model, at a wind speed of around 32 m/s, resulting in a Reynolds number of 250.000, based on the hydraulic diameter and free stream velocity. This matches the Reynolds number of the previous experiments. The train model used in the wind tunnel was a 1.5 car train model, with a dummy first car, bullet head and the optimized head as the tail. Bogie skirts were mounted on the last bogie. The train was mounted on a single track ballast and rail (STBR) and a splitter plate. The tail of the train is painted black in order to reduce the reflections when performing PIV measurements.

To mimic the effect of a long train, an alternate configuration with using a tripping device was also tested, in which a spike strip was mounted to investigate the effect of the boundary layer thickness which is growing with increasing train length on the wake flow pattern (see Figure 17).



Figure 19: The configuration with the spikes installed on the dummy car.

Four different measurement techniques were used to measure and visualize the flow behind the train model: PIV (Particle Image Velocimetry), an omniprobe connected to a traversing system, scanivalves and paint visualization. A high energy pulsating laser and two high-speed cameras were used to capture the flow field behind the train model using PIV. In addition to PIV, the velocity in the wake was also measured with a 12-hole omniprobe mounted on a traversing system. The omniprobe measures all three components of the velocity, including the direction of the flow.



Figure 20: Pictures of the traversing system (left) and omniprobe (right). The omniprobe is placed in the (0,0) position in the right figure, such that the middle of the sphere is aligned to the tip of the tail.

The measurement points were chosen to map the TSI measurement position, to match the measured points of the previous experiments and to visualize the flow structures in the wake. Further, a scanivalve with 10 pressure probe (+1 prandtl tube for reference pressure) was used to measure the boundary layer on the side and on top of the train, just upstream of the tail. In order to visualize the separation over the tail section, paint visualization was used.

The velocities were both measured with PIV and the omniprobe, as explained earlier. The PIV measurements give the two velocity components u, v in the measured plane, while the omniprobe measures all three velocity components at single points.

The results on the new train model from the numerical simulation are compared to the wind tunnel results in Figure 21. Figure 21 shows the contours of streamwise velocity and yz -vectors of the mean flow in three different YZ -planes. The vectors rotate in opposite directions around one point on each side. This motion means that there are two counter-rotating vortices, and the point is the core of each vortex. This core can also be seen in the contours of the u -component. There are many similarities between the CFD and experiments. The contour levels show the same behaviour and the size of the structures are similar. However, in the experiments the flow structures are much closer to the ground than for CFD. For all three cases the core of the counter-rotating vortices are above $z=0.5$ m for the numerical study and below $z=0.5$ m for all the experiments. This means that the flow structures are pulled downwards by the stationary ground. It is an important conclusion and needs to be considered when comparing CFD and experiments at specific heights throughout this paper. Even though the flow is not exactly the same when using a stationary ground, the dominant flow structure is correctly predicted.

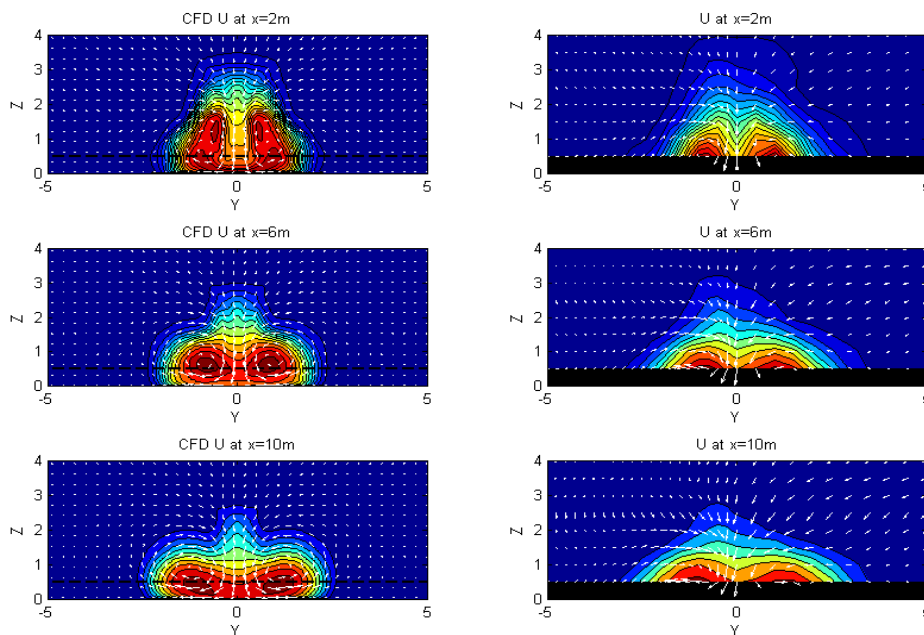


Figure 21: Contour levels of the stream wise component in YZ -planes from omniprobe measurements and CFD computations. The arrows indicate the v, w components. The omniprobe could only measure down to 0.5m above TOR.

The results can also be compared by investigating the velocity contours in XY -planes, which for the experiments are given by the PIV measurements. Figure 22 shows the contours of mean u and u_{rms} for both the experiments and the numerical simulation. It is evident that there are many similarities, the size of the wake is approximately the same and the shapes of many contour levels are very similar. However, there are subtle difference in the contour shapes for the mean U velocity and the strength of the u_{rms} . This is due to the downwards push of the flow structures of the stationary ground, discussed earlier. More slices are shown in the Appendix.

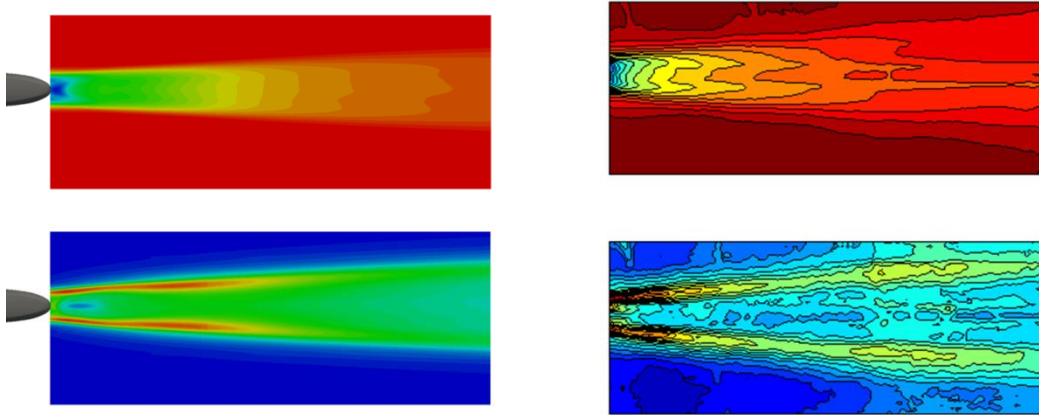


Figure 22: Mean streamwise velocity and streamwise RMS velocity at $Z=0.2$ (full scale) for CFD (left) and PIV (right). The tail of the vehicle is indicated by the grey surface. The contour levels have been removed for confidentiality.

The velocity profiles are plotted across the wake for a fixed streamwise position and multiple heights in Figure 23. This figure shows both numerical and experimental results the results for the optimized train geometry and CRH1. Hence, it is possible to compare the width and velocity of the wake for the different vehicles. The first thing that is evident is that the CFD predicts higher values of the magnitude of the velocity of the wake, relative to the experiments. This is due to the stationary ground in the experiments. Further, the experiments and numerical simulation show the same trend between the optimized geometry and the CRH1, which is that the velocity is higher for the CRH1 than for the optimized geometry. Regarding the width of the wake, the experiments predict that the wake behind the CRH1 is broader at all heights, and the wake is approximately 6 m wide at 1 m above TOR for the optimized head design and about 8 m wide for the CRH1. This is also important for the slipstream behaviour of the two vehicles, since a narrower wake does not affect the sides of the trains as much as a broad wake. For instance, the TSI measurement position is at 3 m from the centre of track and at this distance from the train and only for CRH1 high streamwise velocities occur at this position.

The boundary layer profiles both on the top and side of the train are shown for the two cases, with and without the spike strip in Figure 24. It is interesting to note that the boundary layer profiles are very similar between the two locations for both geometries. The two configurations show a large difference in δ_{99} , which is a measure for the boundary layer thickness. The boundary layer thickness is approximately 35 mm without the spikes and 75 mm with the spikes. This shows that the spike strip has the desired effect and creates a thicker boundary layer in order to mimic a long train.

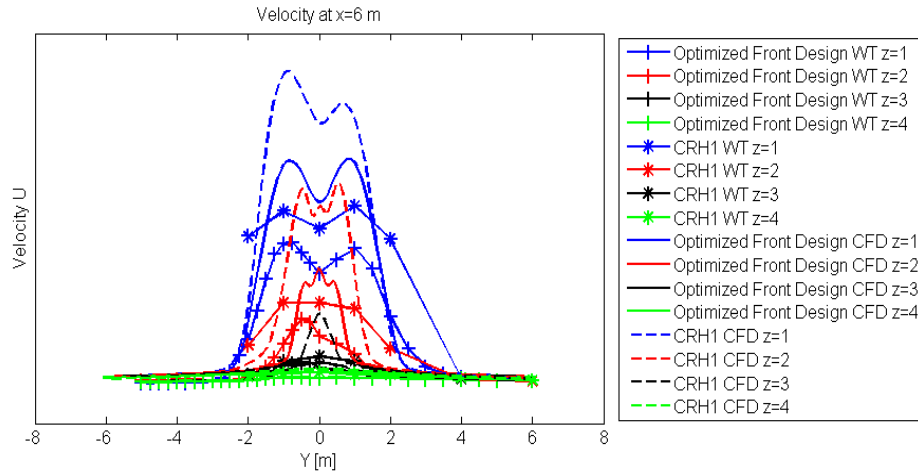


Figure 23: The stream wise velocity at $x=6m$, each line corresponds to a specific height across the wake. The results are given for both the train model and the CRH1, from numerical (CFD) and the current wind tunnel measurements (WT).

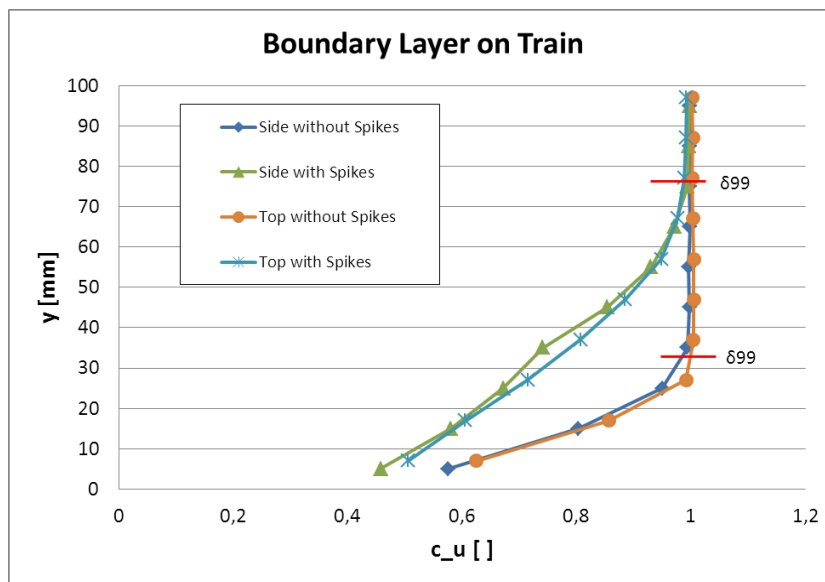


Figure 24: Mean velocity profile in the boundary layer on top and on the side of the train for both the configurations with and without spikes.

This has an impact on the wake flow. The contours of mean u -velocity and u_{rms} are shown in Figure 25, both with and without the spike strip. The difference in the wake flow is quite small, both u -mean and u_{rms} have similar contour shapes for both configurations. However, it appears that the magnitude of u_{rms} is higher close to the train with the spikes. The reason for the asymmetry, for the configuration without spikes, is the inflow condition, which seem to be less pronounced with the spike strip.

Figure 25 Contour of mean u -velocity (top) and u_{rms} velocity (bottom) of the configurations without spikes (left) and

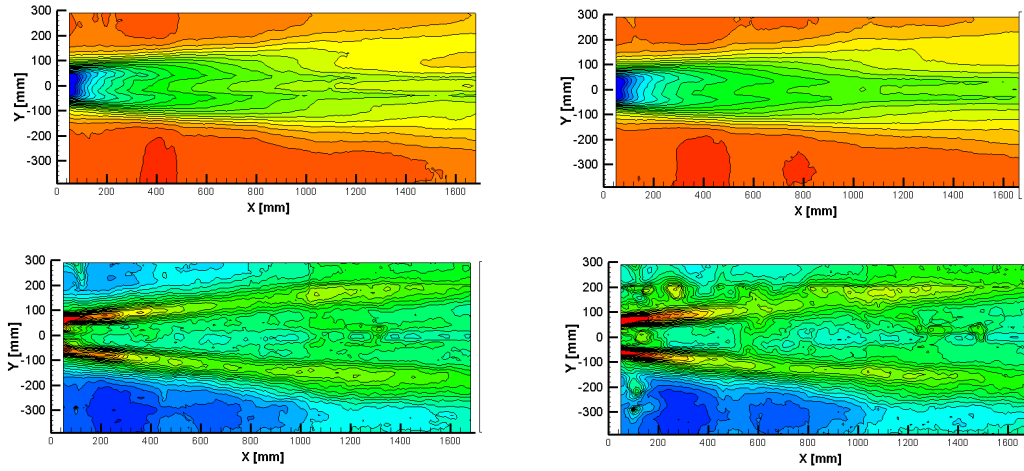


Figure 26: Contour of mean u -velocity (top) and u_{rms} velocity (bottom) of the configurations without spikes (left) and with spikes (right). The contours are shown in the XY-plane at the TSI trackside measurement height. The contour levels have been removed for confidentiality.

6. Conclusions

As a result of the project, increased the knowledge of the flow in the train's wake and its connection to the front shape and an effective methodology to evaluate the slipstream at the side of the train changes as well as a function of the front structure and train length have been obtained. A methodology for predicting the slipstream is in itself a result and an efficient methodology is a prerequisite for more extensive optimization cycle that takes into account several aerodynamic phenomena, as well as other practical and economic aspects. An efficient optimization cycle has been established in order to take all aspects into account and to optimize early in the design cycle of a train. The project result is contributing to the efficient use of a commercial train with minimal impact on the environment and minimizing energy consumption. The work has also provided an insight into how the TSI requirements induced regarding slipstream affect wide body trains and the demands of the front design as the means.

The high-lights of the project results are:

- A methodology for analysis of the wake flow behind the train and the link between flow structures and the frontal shape.
- Increased knowledge of how the actual length affects both the slipstream patterns and drag. Simulations have been complemented by measurements both on full- and model scale.
- A methodology for the prediction of the slipstream that is as efficient as possible, in order to be included in the design iterations where all requirements related to the front are considered.
- An efficient optimization methodology in order to optimize the performance and take all constraints into account early in the design cycle.
- Derivation of a shape optimized front with respect to the slipstream, drag and pressure distribution around the nose to a wide trains that meets the requirements of the TSI to 250 kph.

Through Bombardier's participation it has been ensured that the current level of knowledge in the industry, obtained by measurements both national and international, was a starting point for the project. Results from measurements under Swedish conditions are brought forth by Bombardier in working on standardization and auditing of TSI. In addition, the knowledge regarding the front design applied to new trains using the effective optimization cycle.

For slipstream the most important region of the flow is the near wake, where the flow is complicated with many different time and space scales. To analyze this complex flow, mode decomposition can be used to extract coherent flow structures. The simulated flow field with DES has proven to be adequate to use for decomposition into POD and DMD modes, by studying the modes extracted around the surface-mounted cube. Two different train geometries, the ATM and the CRH1, and one test case, the surface-mounted cube, as well as three different configurations of the ATM, have been simulated.

For these cases, it is found that the POD and DMD mode contain the same flow structures, but the relative importance of the modes could be different. Reconstructing the flow field is proven to be an intelligent way to visualize the flow structures and is used to identify that the dominant flow structure

behind both the ATM and the CRH1 is vortex shedding. This is despite the fact that the flow topology of these two geometries is different. Behind the CRH1 the flow separates with a separation bubble, while behind the ATM the flow separates forming two counter-rotating vortices. The vortex shedding is also found to be the most important flow structures for slipstream.

The velocity profiles in a ground fixed probe have been extracted in order to investigate the slipstream velocities defined by the TSI. As specified in the TSI, 20 probes are extracted and each is filtered with a 1s time average. The results show a large scatter both in peak position and peak value of each probe. The fact that a wider version of the same train would create higher slipstream velocities is verified by looking at the mean flow at different distances from the train side wall.

Three different lengths of the ATM are simulated in order to investigate the effect of the length on the wake flow structures. It is found that the flow topology and the type of dominant flow structures are equivalent, except for the wave length and frequency of the dominant flow structure. The Strouhal number of the vortex shedding decreases when the momentum thickness before the separation increases.

The flow behind the 1:25 scale train model with the optimized head design as the tail has been measured and visualized using PIV, omniprobe, scanivalves and paint visualization. The results have been compared to previous experiments performed on the CRH1 train model and numerical simulations on both the CRH1 and the new train model. In addition, a spike strip is used in the experiments to mimic the effect of a longer train. In the wake behind the train model, there are two counter-rotating vortices.

The same flow structures are obtained in the experiments and numerical simulation. However, the location of the counter-rotating vortices is closer to the ground for the stationary ground experiments. The longer more streamlined tail of the optimized head design creates smaller slipstream velocities and smaller wake than the shorter blunter tail of the CRH1. This was found both in experiments and numerical simulation. The fact that the optimized head design is optimized for drag also improves the slipstream performance. The spikes mounted on the dummy car increase the size of the boundary layer. However, the measured slipstream velocities are only slightly different to those measured without the spikes. The region of separation is well predicted by the numerical simulations.

Publications

[A] Herbst A. H., Muld T.W. and Efraimsson G., Aerodynamic prediction tools for high-speed trains, *International Journal of Rail Transportation*, 2:1, 50-58, DOI: 10.1080/23248378.2013.878295, 2014.

[B] T. W. Muld Slipstream and Flow Structures in the Near Wake of High-Speed Trains, PhD thesis, KTH Farkost och Flyg, KTH, ISBN 978-91-7501-392-3, 2012.

[C] T.W. Muld, G. Efraimsson and D.S. Henningson, Flow structures around a high-speed train extracted using Proper Orthogonal Decomposition and Dynamic Mode Decomposition, *Computers & Fluids* 57, 87-97, 2012

[D] T.W. Muld, G. Efraimsson and D.S. Henningson, Mode Decomposition and Slipstream Velocities in the Wake of Two High-Speed Trains, Inskickat till *The International Journal of Railway Technology*, 2012.

[E] T.W. Muld, G. Efraimsson and D.S. Henningson, Mode Decomposition of Flow Structures in the Wake of Two High-Speed Trains In: *Proceedings of the First International Conference on Railway Technology: Research, Development and Maintenance*, J. Pombo, (Editor), Civil-Comp Press, Stirlingshire, UK, Paper 156, (2012) doi:10.4203/ccp.98.156

[F] T.W. Muld, G. Efraimsson and D.S. Henningson, Wake Characteristics of High-Speed Trains with Different Lengths, Inskickat till *Journal of Rail and Rapid Transit*, 2012

[G] T.W. Muld, G. Efraimsson and D.S. Henningson, Mode Decomposition on Surface-Mounted Cube Flow, *Turbulence and Combustion* 88(3) 279-310 (2012)

[H] Muld T W, Efraimsson G, Henningson D S, Turbulent Inlet Conditions for the Aerodynamic Train Model, Intern rapport KTH, 2012

[I] Guillou, Florian, CFD Study of the Flow around High-Speed Trains, Master Thesis in Aerodynamics, KTH, 2012

[J] Muld T W, Efraimsson G, Henningson D S, Herbst A H and Orellano A, Analysis of Flow Structures in the Wake of a High-Speed Train, *Aerodynamics of Heavy Vehicles III: Trucks, Buses and Trains*, September 12-17, 2012, Potsdam, Germany

[K] Muld, T.W.: Analysis of Flow Structures in Wake Flows for Train Aerodynamics, Licentiatavhandling, ISBN 978-91-7415-651-5, KTH, 2010.

[L] Muld, T.W., Efraimsson G. and Henningson, D.S., Mode Decomposition of the Flow Behind the Aerodynamic Train Model Simulated by Detached Eddy Simulation, Internal report (2010), TRITA-AVE 2010:28, ISSN 1651-7660.

[M] Kållberg, F.: Optimization of the front shape of a wide body train at higher speeds, Master Thesis in Aerodynamics, KTH, 2010.

[N] Schitthelm, A.: Gröna Tåget – Slipstream measurements at windtunnel. Technical report, Bombardier 2009.

[O] Muld, T. W., Efraimsson, G., Henningson, D.S.: Proper Orthogonal Decomposition of flow structures around a surface-mounted cube computed with Detached-Eddy Simulation, SAE World Congress, SAE 2009-01-0331, SP-2226 Vehicle Aerodynamics, 2009.

[P] Muld, T. W., Efraimsson, G., Henningson, D.S., Herbst, A.H., Orellano, A.: Detached eddy simulation and validation on the aerodynamic train model. Proceedings of Euromech Colloquium 509, Vehicle Aerodynamics, External Aerodynamics of Railway vehicles, Trucks, Buses and Cars, Berlin, Germany, March 24-25, 2009.

[Q] Herbst, A. H., Mauss, J., Heiland, J., Orellano, A.: Shape optimization in train aerodynamics, Proceedings of Euromech Colloquium 509, Vehicle Aerodynamics, External Aerodynamics of Railway vehicles, Trucks, Buses and Cars. Berlin, Germany, March 24-25, 2009.

[R] Herbst, A. H.: Gröna tåget – Optimization with regard to head pressure pulse, Technical report, Bombardier, 2008

[S] Weise, M., Diedrichs, B.: Gröna tåget – Slipstream Measurements, Technical report, Bombardier, 2008

[T] Stiebritz, A.: Aerodynamic certification measurements of high-speed trains of head pressure pulse, Diploma Thesis Work, University of Berlin and Bombardier, 2008.

Exchange of knowledge via conferences, seminars, courses and cooperation

Knowledge was exchanged with respect to shape optimization with the project *“Aerodynamisk optimering av fronten hos höghastighetståg” within Gröna tåget at Chalmers, Göteborg (see regarding that project e.g. Krajnovic (2009) [11])*.

A seminar where the project results and conclusions were discussed in detail in depth with participants from KTH, Monash University (Melbourne, Australia, working on experimental methods regarding slipstream) and Bombardier took place in Hennigsdorf, Germany, 31 Januari 2012.

The project result was presented at Gröna tåget slutseminarium på KTH 26 januari 2012 and at the “Seminar on Nordic Railway technology” at 3-4 oktober i Tammsvik.

The work of Tomas Muld has been presented in connection with receiving his doctoral degree 28 May 2010 at KTH. Tomas Muld has received his PhD degree 13 juni 2012 at KTH. Fakultety opponent was Prof Chris Baker from Birmingham University. The grading committee consisted of Prof Lennart Löfdahl, Chalmers, Prof Per Lötstedt, Uppsala Universitet sa and Dr Dragos Morianu, Volvo Cars.

Tomas Muld presented the work "Mode Decomposition of Flow Structures in the Wake of Two High-Speed Trains" at the First International Conference on Railway Technology: Research, Development and Maintenance, Gran Canaria, Spain, 2012

Tomas Muld presented "Analysis of Flow Structures in the Wake of a High-Speed Train" at the conference Aerodynamics of Heavy Vehicles III: Trucks, Buses and Trains, September 12-17, 2010, Potsdam, Germany.

Astrid Herbst has presented "Aerodynamic optimisation for trains at higher speeds" at Nordiska Seminariet för Järnvägsteknik (NSJ) 2010 in Nynäshamn.

In June 2010 och 2009, results have been shown at Svenska Mekanikdagarna.

The work of Tomas Muld has been presented in connection with the licentiate degree 28 May 2010 at KTH.

The work of Fredrik Kållberg master thesis has been presented in connection with the exam 16 April 2010 at KTH.

Results of the generic case have been presented at the SAE world congress 2009. At Euromech Colloquium 509 have both the results of the computations for the first baseline geometry and the optimization of the front shape with respect to head pressure pulse been presented.

An overview of the work has even been presented at the KTH Computational Science and Engineering årsmöte (KCSE) in December 2009 as well as at Technische Universität München (TUM) in September 2009.

The project results have been presented at the "Gröna tåget" reference group meeting in December 2009.

References

- [1] 2008/57/EG 2008 Commission decision of 21 february 2008 concerning a technical specification for interoperability relating to the "rolling stock" sub-system of the trans-european high-speed rail system.
- [2] Ahmed, S. R., Ramm, G. & Faltin, G. 1984 Some Salient Features Of The Time-Averaged Ground Vehicle Wake. *SAE-Paper 840300*.
- [3] Baker, C., Hemida, H., Iwnicki, S., Xie, G. & Ongaro, D. 2011 Integration of crosswind forces into train dynamics modelling. *Proceedings of the Institution of Mechanical Engineers, Part F: Journal of Rail and Rapid Transit* 225, 154–164.
- [4] Baker, C. J. & Sterling, M. 2009 Aerodynamic Forces on Multiple Unit Trains in Cross Winds. *Journal of Fluids Engineering* 131(10), 371–414.
- [5] Diedrichs, B. 2009 Unsteady Aerodynamic Crosswind Stability of a High-Speed Train Subjected to Gusts of Various Rates. *Proceedings Euromech Colloquium 509: Vehicle Aerodynamics* pp. 39–50.
- [6] Diedrichs, B. 2010 Aerodynamic crosswind stability of a regional train model. *Proceedings of the Institution of Mechanical Engineers, Part F: Journal of Rail and Rapid Transit* 224, 580–591.
- [7] Figura-Hardy, G. I. 2007 RSSB Slipstream Safety - Analysis of existing experimental data on train slipstreams including the effects on pushchairs. *Rail Safety and Standards Board*.
- [8] Fröidh, O. 2012 *Green Train, Basis for a Scandinavian high-speed train concept, Part A*. Stockholm.
- [9] Gil, N., Baker, C. & Roberts, C. 2008 The measurement of train slipstream characteristics using a rotating rail rig. *Proceedings BBAA VI International Colloquium on: Bluff Bodies Aerodynamics & Applications*.
- [10] Hemida, H. & Baker, C. 2011 The calculation of train slipstreams using large-eddy simulation techniques. *Proceedings WCRR 2011*.
- [11] Krajnović, S. 2009 Shape optimization of high-speed trains for improved aerodynamic performance. *Proceedings of the Institution of Mechanical Engineers, Part F: Journal of Rail and Rapid Transit*.
- [12] Lumley, J. L. 1967 The structure of inhomogeneous turbulent flows. *In Atmospheric Turbulence and Radio Wave propagation (A.M. Yaglom and V.I. Tatarsky, eds.)* pp. 166–178.
- [13] Manhart, M. & Wengle, H. 1993 A Spatiotemporal Decomposition of a Fully Inhomogeneous Turbulent Flow Field. *Theoretical and Computational Fluid Dynamics* 5, 223–242.
- [14] Morel, T. 1980 Effect of base slant on flow in the near wake of an axisymmetric cylinder. *Aeronautical Quarterly* 31, 132–147.
- [15] Munson, B. R., Young, D. F. & Okiishi, T. H. 2002 *Fundamentals of Fluid Mechanics, 4th Edition*. John Wiley & Sons, USA.
- [16] Rowe, A., Fry, A. L. A. & Motallebi, F. 2000 Influence of Boundary-Layer Thickness on Base Pressure and Vortex Shedding Frequency. *AIAA Journal* 39(4), 754–756.

- [17] Rowley, C. W., Mezić, I., Bagheri, S., Schlatter, P. & Henningson, D. S. 2009 Spectral analysis of nonlinear flows. *Journal of Fluid Mechanics* 641, 115–127.
- [18] Sagaut, P., Deck, S. & Terracol, M. 2006 *Multiscale and Multisolution Approaches in Turbulence*. Imperial college press, Singapore.
- [19] Schetz, J. A. 2001 Aerodynamics of high-speed trains. *Annual Review of Fluid Mechanics* 33, 371–414.
- [20] Schmid, P. J. 2010 Dynamic mode decomposition of numerical and experimental data. *Journal of Fluid Mechanics* 656, 5–28.
- [21] Spalart, P. R., Deck, S., Shur, M. L., Squires, K. D., Strelets, M. K. & Travin, A. 2006 A new version of detached-eddy simulation, resistant to ambiguous grid densities. *Theoretical and Computational Fluid Dynamics* 20, 181–195.
- [22] Spalart, P. R., Jou, W.-H., Strelets, M. & Allmaras, S. R. 1997 Comments on the feasibility of LES for wings, and on a hybrid RANS/LES approach. *First AFOSR International Conference on DNS/LES*.
- [23] Sterling, M., Baker, C. J., Jordan, S. C. & Johnson, T. 2008 A study of the slipstreams of high-speed passenger trains and freight trains. *Proceedings of the Institution of Mechanical Engineers, Part F: Journal of Rail and Rapid Transit* 222, 177–193.
- [24] Weise, M., Schober, M. & Orellano, A. 2006 Slipstream Velocities Induced by Trains. *Proceedings of the 4th WSEAS International Conference on Fluid Mechanics and Aerodynamics* pp. 26–28.